Reviews in Mineralogy & Geochemistry
Vol. 57, pp. 69-104, 2005

Polysomatic Aspects of Microporous Minerals – Heterophyllosilicates, Palysepioles and Rhodesite-Related Structures

Giovanni Ferraris[1,2] and Angela Gula[2]

[1]*Dipartimento di Scienze Mineralogiche e Petrologiche*
Università di Torino
10125 Torino, Italy

[2]*Istituto di Geoscienze e Georisorse*
Consiglio Nazionale delle Ricerche
10125 Torino, Italy

giovanni.ferraris@unito.it *angela.gula@uito.it*

INTRODUCTION

Several structural families reported in this book can be described by using concepts of modular crystallography (Thompson 1978; Veblen 1991; Merlino 1997; Ferraris et al. 2004). This chapter presents three groups of microporous minerals emphasizing the modular aspects of their crystal structures and the role that modularity plays in correlating different structures as well as structure and properties, namely aspects aimed at an engineering of microporous materials (cf. Rocha and Lin 2005).

The description of a crystal structure as an edifice consisting of complex building modules that occur also in other structures implicitly leads to identify features that are common to a group of compounds. This kind of group can often be expressed as a series of structures that are collinear in composition and cell parameters, information that may be crucial to model unknown structures related to the series, as illustrated by some examples in this chapter.

Biopyriboles (Fig. 1) represent a first and now classical example of modular structures established by Thompson (1978). He showed that the structures of micas, pyroxenes and amphiboles share, according to different ratios, the same modules of mica (*M*) and pyroxene (*P*) and are members of a polysomatic series M_mP_p. The ideal chemical composition and cell parameters of the members of the series are linear functions of the ratio *m*/*p*. The classification of biopyriboles as members of a polysomatic series, a type of series belonging to the wider category of the homologous series (cf. Ferraris et al. 2004), and the consequent discovery of the multiple-chain-width biopyriboles jimthompsonite and chesterite (Veblen and Buseck 1979) dramatically proved the predictive power of these series in terms of structure characterization and modeling. The modeling of carlosturanite

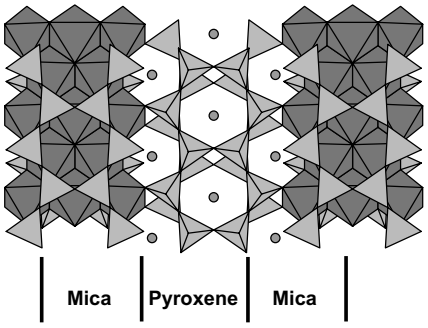

Figure 1. Projection along [100] of the crystal structure of an amphibole showing its slicing as modules of mica and pyroxene.

1529-6466/05/0057-0003$05.00 DOI: 10.2138/rmg.2005.57.3

(Mellini et al. 1985) and of other modular structures reviewed by Veblen (1991) represents some of the earlier successes of polysomatism. These successful examples opened a prolific route as shown by comprehensive reviews in Merlino (1997) and Ferraris et al. (2004). Among other purposes, some microporous structures described in this chapter further clarify the mechanism that is behind the definition of polysomatic and related series.

All the structures described in this chapter contain silicate tetrahedra, which are grouped in sheets and/or strips, and condensed or isolated octahedra. Thus, these structures belong to the larger category of the heterosilicates described in this volume by Chukanov and Pekov (2005) and Rocha and Lin (2005).

The porous properties of the structures here presented are well documented and technologically applied in same cases (e.g., palygorskite and sepiolite); they are instead to some extent speculative in other cases (e.g., members of the heterophyllosilicate series). In the latter case, the structures are discussed with the aim of attracting the attention of those materials scientists who are looking for novel potentially useful porous structures. In particular, the structural parallelism between the 2:1 layer silicates, like micas, and members of the heterophyllosilicate polysomatic series leads to speculate on the possible use of some of these compounds as starting material to produce pillared porous structures analogous to the technologically important pillared clays (cf. Corma 1997). A main problem to be solved on this route is the synthesis of the mineral analogues, not only to have simple and defined chemical compositions, but also because most heterophyllosilicates are quite rare in nature (cf. Khomyakov 1995). Exceptions are astrophyllite, lamprophyllite and, to a minor extent, lomonosovite and murmanite. In the Khibina and Lovozero massifs, lamprophyllite reaches 1–4% as component of lujavrites and is a common accessory mineral in khibinites; lomonosovite and murmanite can be locally considered rock-forming minerals in some formations of the Lovozero massif (N.V. Chukanov, personal communication).

HETEROPHYLLOSILICATES

Octahedral *O* close-packing sheets with full (brucite-type) or partial (e.g., gibbsite-, spinel-, and corundum-type) occupancy of the octahedral sites are recurrent in modular structures. In particular, coupling of a tetrahedral silicate *T* sheet with a dioctahedral (gibbsite) or trioctahedral (brucite) *O* sheet constitutes the building blocks of *TO* (or 1:1) and *TOT* (or 2:1) layer silicates (or phyllosilicates; Fig. 2). For example, the 2:1 layer silicates can be grouped in an A_nB_m merotype series[1] where the *TOT* module (*A*) is the fixed building module and *B* is an interlayer variable module. Talc is representative of $n = 1$ and $m = 0$; micas (*B* = alkaline or alkaline-earth cation), chlorites (*B* = octahedral sheet), and smectites (*B* = alkaline or alkaline-earth cation, H_2O, □) are well known members of the series with $n = 1$ and $m = 1$.

Strips (modules) of *TOT* layers occur in several silicate structures: biopyriboles (Fig. 1), heterophyllosicates and palysepioles (see below for the definition of the two latter groups). This section reports the description of a wide family of layer titanosilicates (heterophyllosilicates) that bear features very close to the *TOT*-based phyllosilicates from which they can be formally derived. In Russian literature, heterophyllosilicates are often referred to as titanosilicate micas and, more generally, as amphoterosilicates (cf. Khomyakov 1995 and Chukanov and Pekov

[1] According to Makovicky (1997), in a merotype series, whereas one building module is kept constant, a second (third, etc.) module is peculiar of each member. A series is said to be plesiotype when all members share modules that, however, may still slightly differ in chemistry and configuration: see the mero-plesiotype series of bafertisite and rhodesite described later in this chapter and other examples in Ferraris et al. (2004).

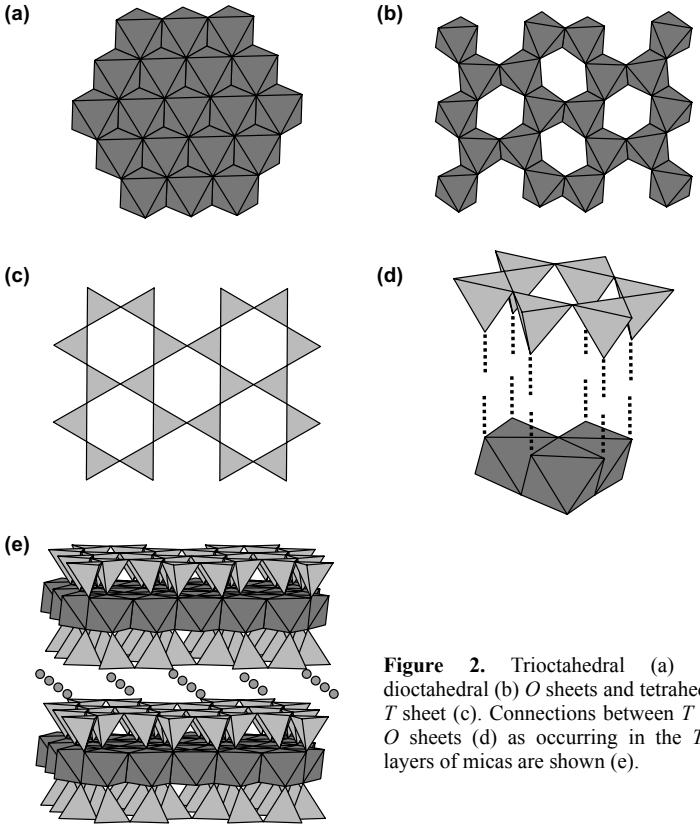

Figure 2. Trioctahedral (a) and dioctahedral (b) *O* sheets and tetrahedral *T* sheet (c). Connections between *T* and *O* sheets (d) as occurring in the *TOT* layers of micas are shown (e).

2005). This term alludes to the fact that the cation Ti^{4+} participates[2], together with Si, in building a mixed tetrahedral/octahedral framework (or just layers), which acts as a complex anion. In its turn, this complex anion hosts in its cavities a variety of cations, including the octahedral ones already present in the anionic part; thus, these cations are said to be "amphoteric."

Polysomatism in the heterophyllosilicates

The characterization of nafertisite, a rare titanosilicate first reported from the Khibina hyperalkaline massif (Kola Peninsula, Russia; Khomyakov et al. 1995) and later from the Igaliko nepheline syenite complex (South Greenland; Petersen et al. 1999)[3], prompted Ferraris et al. (1996, 1997) to correlate a group of titanium silicates whose structures are based on *TOT*-like layers and to introduce the term *heterophyllosilicate*. This correlation has been established via the definition of the polysomatic series of the heterophyllosilicates. In the members of this series, a row of Ti polyhedra (or substituting cations, see footnote 2) periodically substitutes a row of disilicate tetrahedra (silicate diorthogroups) in the *T* tetrahedral sheet that is typical of the layer silicates; the octahedral *O* sheet is instead maintained (Fig. 3). *HOH* layers are thus

[2] Ti^{4+} is the main central cation in these polyhedra, but often it is partially substituted by Nb^{5+}, Zr^{4+} and Fe^{3+} (Tables 1 and 2). Sometimes the latter cations are dominating on Ti, like Zr in seidozerite, Fe in orthoericssonite and Nb in vuonnemite. In the text, for short, only Ti is indicated as centering the relevant polyhedra.

[3] According to N.V. Chukanov (pers. comm.), the IR spectra of samples from the two localities quoted in the text show some differences likely related to cation ordering and other details of the crystal structure.

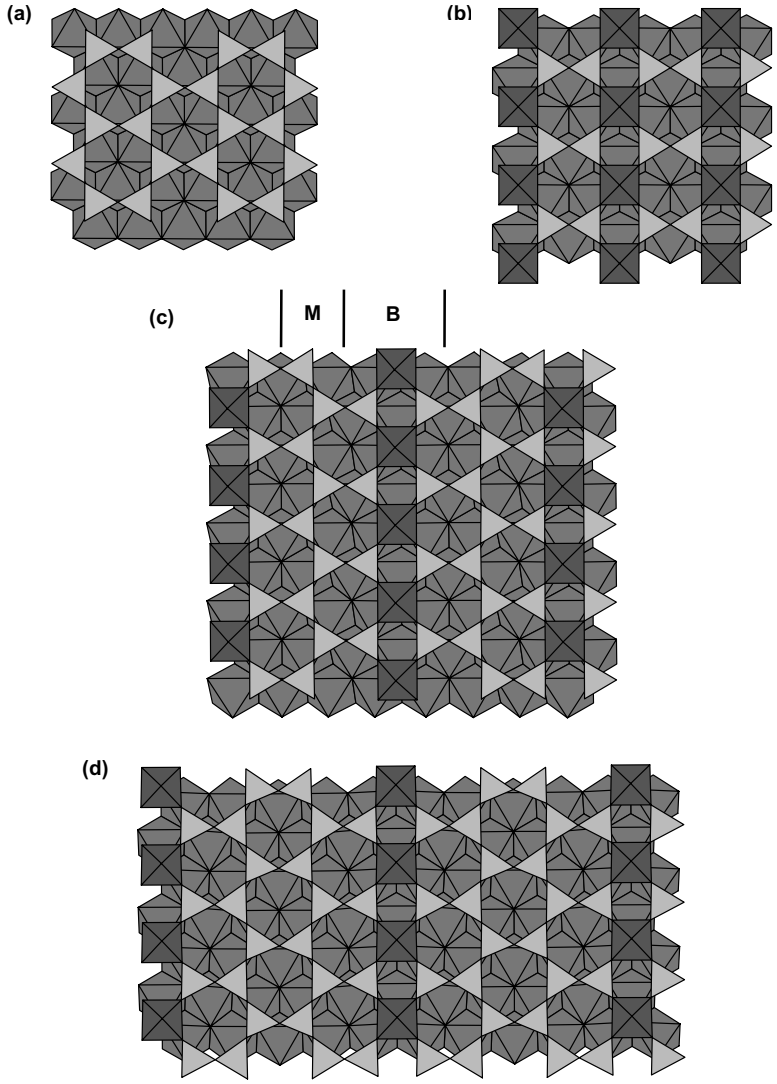

Figure 3. *TOT* layer of a phyllosilicate (a) as transformed, by periodic substitution of rows of octahedra (dark grey) for tetrahedra, to *HOH* heterophyllosilicate layers typical of bafertisite (b), astrophyllite (c) and nafertisite (d). *B* bafertisite-type and *M* mica-type modules are shown in (c).

obtained where *H* stands for *hetero* to indicate the presence of rows of 5- or 6-coordinated Ti in a sheet corresponding to the *T* sheet of the layer silicates. The length of the O···O edges (~ 2.7 Å) of the substituting polyhedra is very close to that of the same edges in the substituted tetrahedra, thus the insertion of the polyhedra in a *T* sheet does not produce strain.

As summarized by Ferraris (1997), depending on the periodicity of the Ti substitution and ignoring some minor topological features, three types of *HOH* layers (Fig. 3) are known so far. The slice of *HOH* layer containing rows of Ti polyhedra in its *H* sheet is conventionally called bafertisite-type module and has composition $B = I_2Y_4[X_2(O)_4Si_4O_{14}](O,OH)_2$; this module may

be intercalated with a mica-type module $M = IY_3[Si_4O_{10}](O,OH)_2$. In the two formulae, *I* and *Y* represent interlayer and octahedral cations, respectively; *X* corresponds to Ti and its vicariant elements as stated in footnote 2.

$(HOH)_B$ *bafertisite-type layer*. In this layer, a bafertisite-type module alone is periodically repeated (Fig. 3). The heterophyllosilicates based on the resulting $(HOH)_B$ layer are some tens and are described in a subsequent section as the mero-plesiotype bafertisite series. We shall see, however, that in this series the so-called bafertisite-type layer does actually correspond to two topologically different modules. Anyway, if it is not necessary to specify, the undifferentiated layer is indicated as $(HOH)_B$. As discussed in the section on the rhodesite group of structures, a *H* bafertisite-type sheet occurs also in the structure of jonesite (Krivovichev and Armbruster 2004).

$(HOH)_A$ *astrophyllite-type layer*. Relative to the $(HOH)_B$ layer, in a $(HOH)_A$ astrophyllite-type layer a one-chain-wide mica-like module *M* is present between two bafertisite-type modules (Fig. 3). As recently discussed by Piilonen et al. (2003a,b), the known heterophyllosilicates based on a $(HOH)_A$ layer form a complex isomorphous series (Table 1) and mineral species are defined by the chemical nature of *I*, *Y* and *X* cations in the formula given above; some polytypes are known. As mentioned above, astrophyllite is one of the few non-rare heterophyllosilicates. Except in magnesium astrophyllite (Shi et al. 1998), in these structures the layers are locked together by sharing an oxygen atom between two Ti (*X* cation) octahedra belonging to adjacent layers (Fig. 4). Thus, [100] channels are realized with windows characterized by a small (~ 1.5 Å) minimum effective width[4]. Chelishchev (1972, 1973) has proved that under supercritical conditions (400–600°C; pressure of 1000 kg/cm^2) astrophyllite exchanges K with Na, Rb and Cs; anyway, this group of heterophyllosilicates will no longer be considered in this chapter.

Eveslogite. $\{(Ca,K,Na,Sr,Ba)_{48}[(Ti,Nb,Fe,Mn)_{12}(OH)_{12}Si_{48}O_{144}](F,OH,Cl)_{14}$; *P*2/*m*, $a = 14.069$, $b = 24.937$, $c = 44.31$ Å, $\gamma = 95.02°\}$ is a titanosilicate recently described from Khibina massif (Men'shikov et al. 2003). It shows an *ab* base 6-times larger than that of astrophyllite and 3-times larger than that of magnesium astrophyllite (Table 1). Its *c* parameter corresponds to the thickness of four $(HOH)_A$ astrophyllite-type layers. On this basis, it was suggested (cf. Ferraris et al. 2004) that the crystal structure of eveslogite is based on a [001] stacking of four $(HOH)_A$ layers. That supports a fitting of the eveslogite chemical data to an astrophyllite-like chemical formula. However, according to IR data (N.V. Chukanov, personal communication) the crystal structure of eveslogite is likely close to that of yuksporite $[(Sr,Ba)_2K_4(Ca,Na)_{14}(□,Mn,Fe)\{(Ti,Nb)_4(O,OH)_4[Si_6O_{17}]_2[Si_2O_7]_3\}(H_2O,OH)_n$; $a = 7.126$, $b = 24.913$, $c = 17.075$ Å, $\beta = 101.89°$; $P2_1/m$], a mineral from Khibina massif to which Men'shikov et al. (2003) tentatively assigned a layer structure, together with eveslogite. Recently, Krivovichev et al. (2004) have instead shown that yuksporite has a microporous structure based on [100] channels delimited by Si tetrahedra and Ti octahedra.

$(HOH)_N$ *nafertisite-type layer*. Relative to the $(HOH)_B$ layer, in a $(HOH)_N$ nafertisite-type layer two one-chain-wide mica-like modules *M* are present between two bafertisite-type modules [Fig. 3; alternatively, one can say that a second *M* module is intercalated in the $(HOH)_A$ astrophyllite-type layer].

Nafertisite $\{nfr$; $(Na,K,□)_4(Fe^{2+},Fe^{3+},□)_{10}[Ti_2O_3Si_{12}O_{34}](O,OH)_6$; *A*2/*m*, $a = 5.353$, $b = 16.176$, $c = 21.95$ Å, $\beta = 94.6°\}$ is the only compound known to be based on a $(HOH)_N$ layer. No single crystals suitable for X-ray diffraction analysis are available; a model of the

[4] The minimum effective width is calculated as the minimum O···O distance across the interlayer minus the ionic diameter of O^{2-} (2.7 Å; McCusker et al. 2003).

Table 1. Members of the astrophyllite group. Space groups are shown in agreement with the following choice of axes: $a \sim 5.4$ and $b \sim 11.9$ Å (or multiples) in the *HOH* layer; $c \sim 11.7$ Å (or multiple) outside the layer.

Name	*Chemical Formula*	*Space group*
Niobokupletskite	$K_2Na\{(Mn,Zn,Fe)_7[(Nb,Zr,Ti)_2O_3Si_8O_{24}](O,OH,F)_4\}$	$P\bar{1}$
Kupletskite-1*A*	$K_2Na\{(Mn,Fe^{2+})_7[(Ti,Nb)_2(O_2F)Si_8O_{24}](OH)_4\}$	$P\bar{1}$
Kupletskite-*Ma2b2c*	$K_2Na\{(Mn,Fe^{2+})_7[Ti_2(O_2F)Si_8O_{24}](OH)_4\}$	$C2/c$
Kupletskite-(Cs) [c]	$(Cs,K)_2Na\{(Mn,Fe,Li)_7[(Ti,Nb)_2(O_2F)Si_8O_{24}](OH)_4\}$	?
Astrophyllite	$K_2Na\{(Fe^{2+},Mn)_7[Ti_2(O_2F)Si_8O_{26}](OH)_4\}$	$A\bar{1}$
Magnesium astrophyllite [a]	$K_2Na\{[Na(Fe,Mn)_4Mg_2][Ti_2O_2Si_8O_{24}](OH)_4\}$	$C2$
Niobophyllite	$K_2Na\{(Fe^{2+},Mn)_7[(Nb,Ti)_2(F,O)_3Si_8O_{24}(OH)_4\}$	$P\bar{1}$
Zircophyllite [c]	$K_2(Na,Ca)\{(Mn,Fe^{2+})_7[(Zr,Nb)_2(O_2F)Si_8O_{24}](OH)_4\}$	?
Fe-dominant zircophyllite [b, c]	$K_2(Na,Ca)\{(Fe^{2+},Mn)_7[(Zr,Nb)_2(O_2F)Si_8O_{24}](OH)_4\}$	?
"Hydroastrophyllite" [b, c]	$(H_3O,K)_2Ca\{(Fe^{2+},Mn)_{5\text{-}6}[Ti_2(O_2F)Si_8O_{24}](OH)_4\}$	?

[a] Ti is 5 coordinated (see Fig. 4b).
[b] Not approved as mineral species.
[c] Structure unknown.

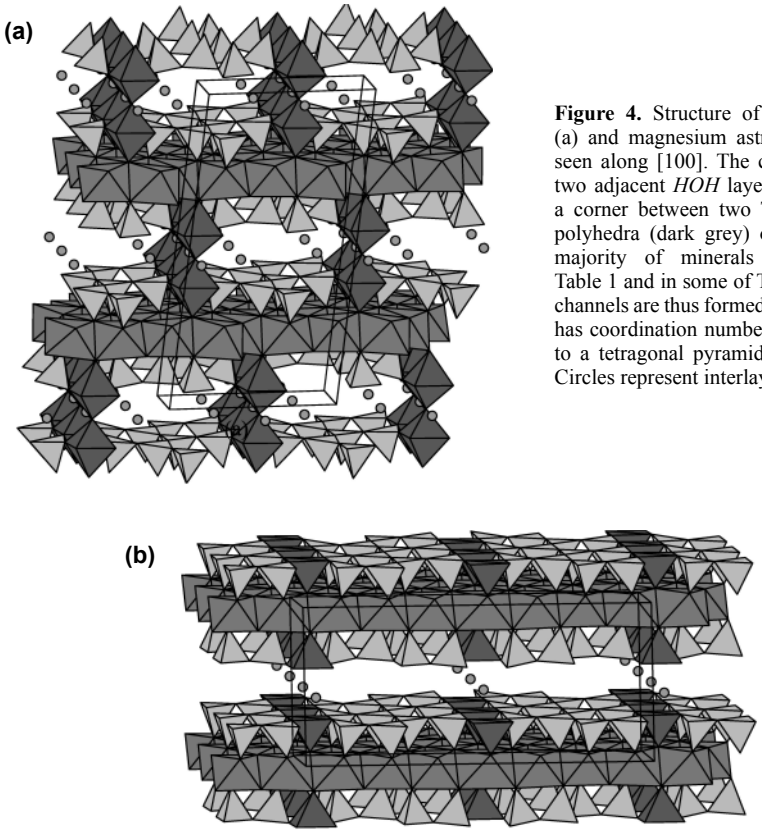

Figure 4. Structure of astrophyllite (a) and magnesium astrophyllite (b) seen along [100]. The connection of two adjacent *HOH* layers by sharing a corner between two Ti (*X* cation) polyhedra (dark grey) occurs in the majority of minerals reported in Table 1 and in some of Table 2: [100] channels are thus formed (a). In (b), Ti has coordination number 5 according to a tetragonal pyramid (dark grey). Circles represent interlayer cations.

crystal structure of nafertisite was obtained (Ferraris et al. 1996) by comparing its chemical composition and cell parameters with those of:

- bafertisite {*bft*; $Ba_2(Fe,Mn)_4[Ti_2O_4Si_4O_{14}](O,OH)_2$; $P2_1/m$, $a = 5.36$, $b = 6.80$, $c = 10.98$ Å, $\beta = 94°$; Pen and Shen (1963); see a discussion in the section 'Pseudosymmetries'};
- astrophyllite {*ast*; $(K,Na)_3(Fe,Mn)_7[Ti_2O_3Si_8O_{24}](O,OH)_4$; $P\bar{1}$, $a = 5.36$, $b = 11.63$, $c = 11.76$ Å, $\alpha = 112.1$, $\beta = 103.1$, $\gamma = 94.6°$; *P*, instead of the *A* cell of Woodrow (1967), is here adopted}.

The following observations allowed to build a model of the structure of nafertisite by inserting a further *M* mica-type module in the *HOH* layer of astrophyllite (Fig. 5).

a. The difference in composition between astrophyllite and nafertisite is about $(I,\square)(Y,\square)_3[Si_4O_{10}](OH,O)_2$; it is comparable to the composition of an *M* mica-type module and corresponds to half the difference between the compositions of nafertisite and bafertisite.

b. Bafertisite, astrophyllite and nafertisite have a common value of $a \sim 5.4$ Å, which matches the *a* value of mica.

c. The value of the differences $(b_{ast} - b_{bft}) \sim 1/2(b_{nfr} - b_{bft}) \sim 4.7$ Å corresponds to the value of $b/2$ in mica; $(d_{002})_{nfr} = 10.94$ Å matches the thickness of one *HOH* layer in bafertisite and astrophyllite.

In the structure of nafertisite, the layers are locked together via sharing an oxygen atom between two Ti octahedra that belong to adjacent layers (Fig. 5). Thus, the interlayer space is subdivided in [100] channels with a small effective width like that mentioned for astrophyllite.

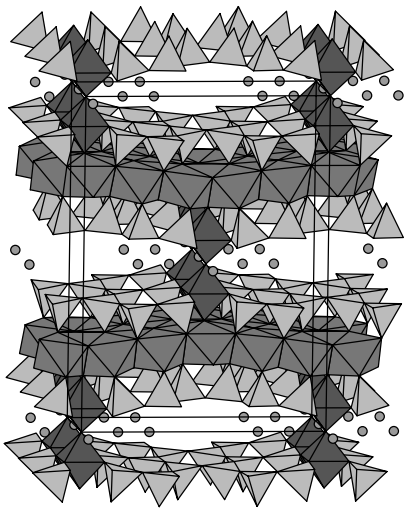

Figure 5. View along [100] of the crystal structure of nafertisite. Pairs of Ti polyhedra (dark grey) share a corner across the interlayer space, thus forming [100] channels. Circles as in Figure 4.

The heterophyllosilicate polysomatic series. Following the description given above, bafertisite, astrophyllite and nafertisite are members of a B_mM_n polysomatic series with general formula $I_{2+n}Y_{4+3n}[X_2(O')_{2+p}Si_{4+4n}O_{14+10n}](O'')_{2+2n}$. In this formula, atoms belonging, even in part, to the *H* sheet are shown in square brackets. *I* represents large (alkali) interlayer cations and *Y* octahedral cations; O' (bonded to *X*) and O'' (belonging to the octahedral sheet only) can be an oxygen atom, OH, F or H_2O; the $14+10n$ oxygen atoms are bonded to Si. The *X* cation is 5- or 6-coordinated according to polyhedra that share one corner with the octahedral sheet and four corners with four Si tetrahedra of the *T* sheet. The value of *p* (0, 1, 2) depends on the configuration around *X*. In case of octahedral coordination, the sixth corner can be (i) unshared ($p = 2$), (ii) shared with an octahedron of the adjacent layer ($p = 1$) or (iii) with an interlayer anion ($p = 0$); $p = 0$ holds also when (iv) an edge is shared between two octahedra or (v) the coordination number of *X* is 5 (see below figures with examples). In the cases (ii) and (iv) a "layered" framework structure is actually formed.

The heterophyllosilicates have also been described by using differently defined modules (Christiansen et al. 1999), a possibility which is not rare in modular crystallography.

Heterophyllosilicates vs. porosity. Layer structures like heterophyllosilicates cannot be included in the definition of "ordered microporous and mesoporous materials" adopted by IUPAC (McCusker et al. 2003; McCusker 2005). That because, even if wide enough to allow exchange of at least water molecules, in these structures the interlayer space extends in two dimensions, namely microporosity does not develop according to specific ordered spaces corresponding to channels, cages and cavities.

Actually, as mentioned above, some heterophyllosilicates show the interlayer space subdivided in channels by bridges established via polyhedra that share corners, thus locking together the layers; however, the minimum effective width of these channels is below or at the bottom scale of porosity. Subdivision of the interlayer space is observed also in several so-called modulated phyllosilicates (cf. Guggenheim and Eggleton 1988), namely those silicates where a periodic perturbation to the basic layer structure occurs (see Section on Palysepioles below).

Both the heterophyllosicates with locked layers and the mentioned modulated phyllosilicates actually show a framework structure, although usually they are considered "layered structures" because condensation of polyhedra in layers is an outstanding structural feature. In particular, the heterophyllosilicates with locked layers can be considered a transition structural type between true layer titanosilicates and framework titanosilicates extensively described in this volume by Chukanov and Pekov (2005) and Pekov and Chukanov (2005).

The main interest to consider heterophyllosilicates here is however related to a hypothesis of using their layers as starting modules to build pillared materials, another kind of porous structures defined (Schoonheydt et al. 1999) separately from the ordered porous structures mentioned above.

The bafertisite series

The $(HOH)_B$ bafertisite-type layer is the most versatile of the three heterophyllosilicate layers defined above, being able to sandwich a large variety of interlayer contents. The number of crystal structures containing this layer is comparable to that known for structures containing the *TOT* phyllosilicate layer. However, the latter appears in important rock-forming minerals, like micas and clay minerals, while the titanosilicates we are dealing with occur only in rare hyperalkaline rocks (Table 2; Khomyakov 1995).

Two main groups of $(HOH)_B$-bearing compounds are known: the götzenite group, where Ca is at the centre of the hetero-octahedra and is not of interest in this chapter (cf. Christiansen and Rønsbo 2000; Ferraris et al. 2004), and the complex bafertisite series (Ferraris et al. 1997) where the $(HOH)_B$ layer alternates with a large variety of interlayer contents [cf. Egorov-Tismenko and Sokolova (1990) and Egorov-Tismenko (1998) for earlier crystal-chemical analyses of part of the series and quotation of former Russian papers on layer titanosilicates]. The members of this series are related by merotypy to the B_1M_0 member (i.e., bafertisite) of the heterophyllosilicate polysomatic series, in the sense (cf. footnote 1) that whereas the $(HOH)_B$ layer appears in all members, the interlayer content is characteristic of each member. For the members of the bafertisite series the general formula given above becomes $A_2\{Y_4[X_2(O')_{2+p}Si_4O_{14}](O'')_2\}W$; the interlayer content labeled *I* in the general formula is here split into *A* (alkaline and alkaline-earth large cations) and *W* (H_2O molecules and complex anions). In this formula:

1. $[X_2(O')_{2+p}Si_4O_{14}]^{n-}$ is a complex anion representing the heterophyllosilicate *H* sheet alone;
2. $\{Y_4[X_2(O')_{2+p}Si_4O_{14}](O'')_2\}^{m-}$ is a larger complex anion representing the whole $(HOH)_B$ layer; it is within braces that leave outside the interlayer contents *A* and *W* (Table 2).

Table 2. Members of the mero-plesiotype bafertisite series in increasing order of the cell parameter (*t,* Å) (either *c* or *a*) stacking the layers. The content of the heteropolyhedral *H* sheet is shown in square brackets, and that of the *HOH* layer is within braces; the composition of the interlayer is shown outside the braces.

Name	*Chemical formula*	t^{m} (Å)	*Space group*	*Reference* [l]
Murmanite [a]	$(Na,\square)_2\{(Na,Ti)_4[Ti_2(O,H_2O)_4Si_4O_{14}](OH,F)_2\}\cdot 2H_2O$	11.70	$P\bar{1}$	Nèmeth et al. 2005
Bafertisite [a]	$Ba_2\{(Fe,Mn)_4[Ti_2O_2(O,OH)_2Si_4O_{14}](O,OH)_2\}$	11.73	*Cm*	Guan et al. 1963
Hejtmanite [a]	$Ba_2\{(Mn,Fe)_4[Ti_2(O,OH)_4Si_4O_{14}](OH,F)_2\}$	11.77	*Cm*	Rastsvetaeva et al. 1991
Epistolite [b]	$(Na,\square)_2\{(Na,Ti)_4[Nb_2(O,H_2O)_4Si_4O_{14}](OH,F)_2\}\cdot 2H_2O$	12.14	$P\bar{1}$	Nèmeth et al. 2005
Vuonnemite [b]	$Na_8\{(Na,Ti)_4[Nb_2O_2Si_4O_{14}](O,OH,F)_2\}(PO_4)_2$	14.45	$P\bar{1}$	Ercit et al. 1998
Lomonosovite [a, n]	$Na_8\{(Na,Ti)_4[Ti_2O_2Si_4O_{14}](O,OH)_2\}(PO_4)_2$	14.50	$P\bar{1}$	Belov et al. 1978
Synthetic vanadate [a]	$Na_8\{(Na,Ti)_4[Ti_2O_2Si_4O_{14}]O_2\}(VO_4)_2$	14.75	*P*1	Massa et al. 2000
Yoshimuraite [a, c]	$Ba_4\{Mn_4[Ti_2O_2Si_4O_{14}](OH)_2\}(PO_4)_2$	14.75	$P\bar{1}$	McDonald et al. 2000
Innelite [b, c]	$(Ba,K)_2Ba_2\{(Na,Ca,Ti)_4[Ti_2O_2Si_4O_{14}]O_2\}(SO_4)_2$	14.76	*P*1	Chernov et al. 1971
Bussenite [a]	$Ba_4Na_2\{(Na,Fe,Mn)_2[Ti_2O_2Si_4O_{14}](OH)_2\}(CO_3)_2F_2\cdot 2H_2O$	16.25	$P\bar{1}$	Zhou et al. 2002
Seidozerite [b, g, i]	$Na_2\{(Na,Mn,Ti)_4[(Zr,Ti)_2O_2Si_4O_{14}]F_2\}$	18.20	*P*2/*c*	Pushcharovsky et al. 2002
Lamprophyllite [b, c]	$(Sr,Ba)_2\{(Na,Ti)_4[Ti_2O_2Si_4O_{14}](OH,F)_2\}$	19.49	*C*2/*m*	Rastsvetaeva et al. 1990
Nabalamprophyllite [b, c]	$Ba(Na,Ba)\{(Na,Ti,)_4[Ti_2O_2Si_4O_{14}](OH,F)_2\}$	19.74	*P*2/*m*	Rastsvetaeva and Chukanov 1999
Barytolamprophyllite [b, c]	$(Ba,Na)_2\{(Na,Ti)_4[Ti_2O_2Si_4O_{14}](OH,F)_2\}$	19.83	*C*2/*m*	Pen et al. 1984
Orthoericssonite [b, c]	$Ba_2\{Mn_4[Fe_2O_2Si_4O_{14}](OH)_2\}$	20.23	*Pnmn*	Matsubara 1980
Quadruphite [a]	$Na_{13}Ca\{(Ti,Na,Mg)_4[Ti_2O_2Si_4O_{14}]O_2\}(PO_4)_4F_2$	20.36	$P\bar{1}$	Sokolova and Hawthorne 2001

Continued on following page

Table 2 continued from previous page.

Name	*Chemical formula*	t [m] (Å)	*Space group*	*Reference* [l]
Ericssonite [e]	$Ba_2\{Mn_4[Fe_2O_2Si_4O_{14}](OH)_2\}$	20.42	*C*2/*m*	Moore 1971
Surkhobite [a, i]	$(Ca,Na,Ba,K)_2\{(Fe,Mn)_4[Ti_2O_2Si_4O_{14}](F,O,OH)_3\}$	20.79	*C*2	Rozenberg et al. 2003
Jinshajiangite [e, p]	$(Na,Ca)(Ba,K)\{(Fe,Mn)_4[(Ti,Nb)_2O_3Si_4O_{14}](F,O)_2\}$	20.82	*C*2/*m*?	Hong and Fu 1982
Perraultite [a, i]	$(Na,Ca)(Ba,K)\{(Mn,Fe)_4[(Ti,Nb)_2O_3Si_4O_{14}](OH,F)_2\}$	20.84	*C*2	Yamnova et al. 1998
Delindeite [b]	$Ba_2\{(Na,Ti,\square)_4[Ti_2(O,OH)_4Si_4O_{14}](H_2O,OH)_2\}$	21.51	*A*2/*m*	Ferraris et al. 2001b
Polyphite [a]	$Na_{14}(Ca,Mn,Mg)_5\{(Ti,Mn,Mg)_4[Ti_2O_2Si_4O_{14}]F_2\}(PO_4)_6F_4$	26.56	$P\bar{1}$	Sokolova et al. 1987
M55C [e]	$Na_8\{(Na,Ti)_4[Ti_2O_2Si_4O_{14}](O,F)_2\}(PO_4)_2$?	28.1	$P112_1/m$	Nèmeth 2004
Shkatulkalite [e]	$\{(Na,Mn,Ca,\square)_4[(Nb,Ti)_2(H_2O)_2Si_4O_{14}](OH, H_2O,F)_2\}\cdot 2(H_2O,\square)$	31.1	*P*2/*m*	Men'shikov et al. 1996
M55A [e]	$Ba(Na,\square)_5\{(Na_3Ti)[(Ti,Nb)_2O_2Si_4O_{14}](F,OH,O)_2\}(PO_4)_2\cdot 4H_2O$	38.11	$P112_1/m$	Nèmeth 2004[f], Khomyakov 1995
Sobolevite [a]	$Na_{12}CaMg\{(Ti,Na,Mg)_4[Ti_2O_2Si_4O_{14}]O_2\}(PO_4)_4F_2$	40.62	*P*1	Sokolova et al. 1988
M55B [e]	$\{(Na,K,Ba,\square)_4[(Ti,Nb)_2(H_2O,OH)_2Si_4O_{14}](F,H_2O,\square)_2\}$	43.01	$P112_1/m$	Nèmeth 2004
Bornemanite [a, i]	$BaNa_3\{(Na,Ti,Mn)_4[(Ti,Nb)_2O_2Si_4O_{14}](F,OH)_2\}PO_4$	47.95	*Ib*	Ferraris et al. 2001a
M73 [a, d]	$(Ba,Na)_2\{(Na,Ti,Mn)_4[(Ti,Nb)_2(OH)_3Si_4O_{14}](OH,O,F)_2\}\cdot 3H_2O$	48.02	*A*2/*m*	Nèmeth 2004[f], Khomyakov 1995
M72 [a, d, h]	$BaNa\{(Na,Ti)_4[(Ti,Nb)_2(OH,O)_3Si_4O_{14}](OH,F)_2\}\cdot 3H_2O$	50.94	*Im*	Nèmeth 2004[f], Khomyakov 1995

[a] $(HOH)_B$ layer. - [b] $(HOH)_V$ layer. - [c] *X* cation in coordination 5. - [d] *X* cation in coordination 5 and 6. - [e] Structure unknown; the inclusion of the mineral in this table is based mainly on chemical and crystal data. - [f] Crystallographic data. - [g] Grenmarite (Bellezza et al. 2004) is a new species that differs from seidozerite for having Zr dominating also in one site of the *O* sheet. Actually, seidozerite is included in this Table more for historical [see the first introduction of this series by Egorov-Tismenko and Sokolova (1990)] than structural reasons; in fact, sharing of edges between adjacent *HOH* layers and the consequent lack of a real interlayer space suggest the inclusion of seidozerite in the götzenite-rosenbuschite-seidozerite family (cf. Christiansen et al. 2003 and Bellezza et al. 2004) - [h] Approved as mineral species: IMA No 2003-044 (Burke and Ferraris 2004) - [i] Two octahedra of *X* cations share either a corner or an edge – [l] Reference to the most recent paper describing the structure, when known, otherwise to the paper describing the species. [m] The cells given by authors have been converted to reduced cells, if the case. [n] "Betalomonosovite" is a discredited mineral species with composition close to that of lomonosovite; its crystal structure (a = 5.326, b = 14.184, c = 14.47 Å, α = 102.2, β = 95.5, γ = 90.17°; *P*-1, Rastsvetaeva 1998). [p] IR spectra (N. V. Chukanov, personal communication), cell parameters and composition suggest that jinshajingite has the same structure of perraultite thus corresponding to the Fe dominant of the latter mineral.

Structural aspects in the bafertisite series

In the known members of the bafertisite series (Table 2), both the *H* sheet and the whole $(HOH)_B$ layer are negatively charged, thus the more or less complex interlayer content acts as a cation. In some cases, e.g., epistolite, murmanite, M72 and M73, the charge of the layer is very weak, an aspect discussed later. Fixing as *c* the cell parameter outside the $(HOH)_B$ layer, all the heterophyllosilicates listed in Table 2 are characterized by similar values of $a \sim 5.4$ Å and $b \sim 7.1$ Å (or multiples), i.e., of the periodicities within the layer.

The HOH layer. In terms of merotypy and plesiotypy (see footnote 1), the heterophyllosilicates of Table 2 form a mero-plesiotype series (Ferraris et al. 2001b). This series is merotype because the *HOH* module is constantly present in the crystal structure of all members, whereas a second module, namely the interlayer content, is peculiar to each member. At the same time, the series has a plesiotype character because chemical nature and coordination number of the *X* and *Y* cations and the linkage between the *H* and *O* sheets may be modified. In fact, as discussed by Sokolova and Hawthorne (2004) (cf. also Christiansen et al. 1999), the two *H* sheets sandwiching an *O* sheet are either facing each other via the same type of polyhedra (i.e., heteropolyhedra face each other) or showing a relative shift (i.e., a heteropolyhedron faces a tetrahedron), thus realizing two different topologies. The two kinds of *HOH* layer occurring in vuonnemite, $(HOH)_V$, and in bafertisite, $(HOH)_B$, are here considered typical examples of the two topologies (Fig. 6). Besides, the coordination

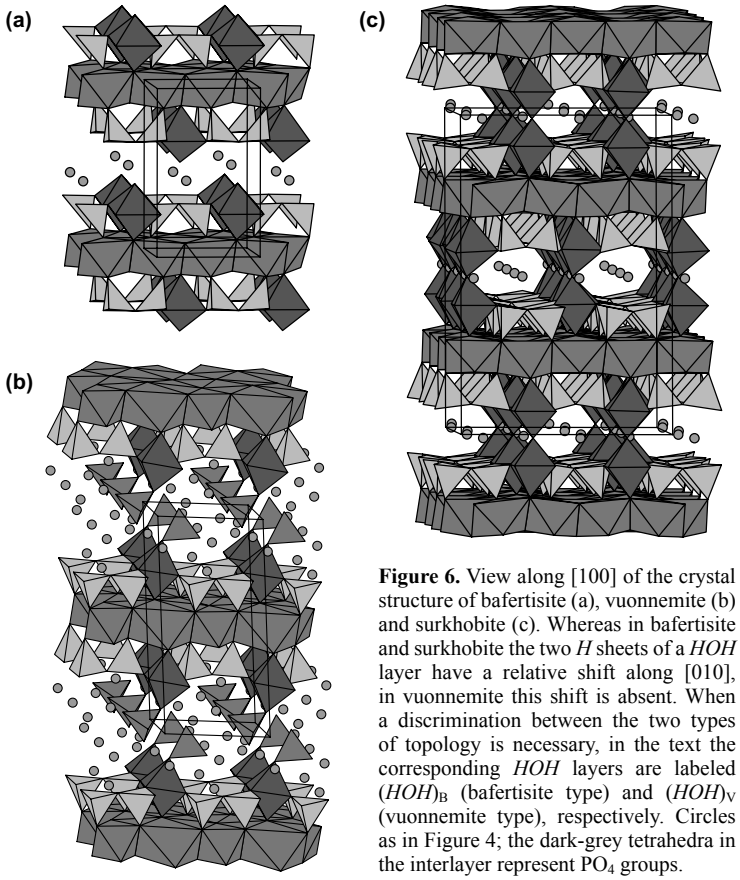

Figure 6. View along [100] of the crystal structure of bafertisite (a), vuonnemite (b) and surkhobite (c). Whereas in bafertisite and surkhobite the two *H* sheets of a *HOH* layer have a relative shift along [010], in vuonnemite this shift is absent. When a discrimination between the two types of topology is necessary, in the text the corresponding *HOH* layers are labeled $(HOH)_B$ (bafertisite type) and $(HOH)_V$ (vuonnemite type), respectively. Circles as in Figure 4; the dark-grey tetrahedra in the interlayer represent PO_4 groups.

number of the *X* cations can be either 5 (square pyramid) or 6 (octahedron); the two types of coordination occur even in the same structure (Figs. 7 and 8). Note that the configuration with coordination 5 is a way to decrease the total negative charge of the *HOH* layer; the same result can be obtained via a higher charge of the *X* cation (e.g., Nb^{5+} instead of Ti^{4+}) or presence of high-charge *Y* cations (e.g., Fe^{3+} and Ti^{4+}).

The $(HOH)_B$ layer is more common (see footnotes *a* and *b* in Table 2). Nèmeth et al. (2005) inferred that the different topology observed for the *HOH* layer in the pair epistolite, $(HOH)_V$, and murmanite, $(HOH)_B$, in spite of their similar chemical composition (Table 2), is likely related to the Na/Ti ratio in the *O* sheet and to the different charge of the *X* cation (either Nb^{5+} of Ti^{4+}). The following reasons, that likely are valid for other members of Table 2, were given. An oxygen atom shared between *H* and *O* sheets is bonded to four cations: three belonging to the *O* sheet and one to the *H* sheet. Because of bond-valence balance, even an O^{2-} anion cannot be bonded at the same time to four high-charge cations like Si^{4+} and Ti^{4+} or Nb^{5+}; consequently, constraints are derived not only to the composition, but also to the topology of the *HOH* layer. Thus, to reach a suitable bond-valence balance, Na octahedra share edges between them in epistolite but not in murmanite and a different connectivity between the *H* and *O* sheets is established.

The interlayer. As does the *TOT* layer in the 2:1 phyllosilicates, in the heterophyllosilicates two adjacent *HOH* modules delimit an interlayer space that contains (Table 2) either a single cation or a complex composition which may even correspond to that of a known mineral, like nacaphite, $Na_2Ca[PO_4]F$ (Sokolova et al. 1989a) occurring in quadruphite, polyphite

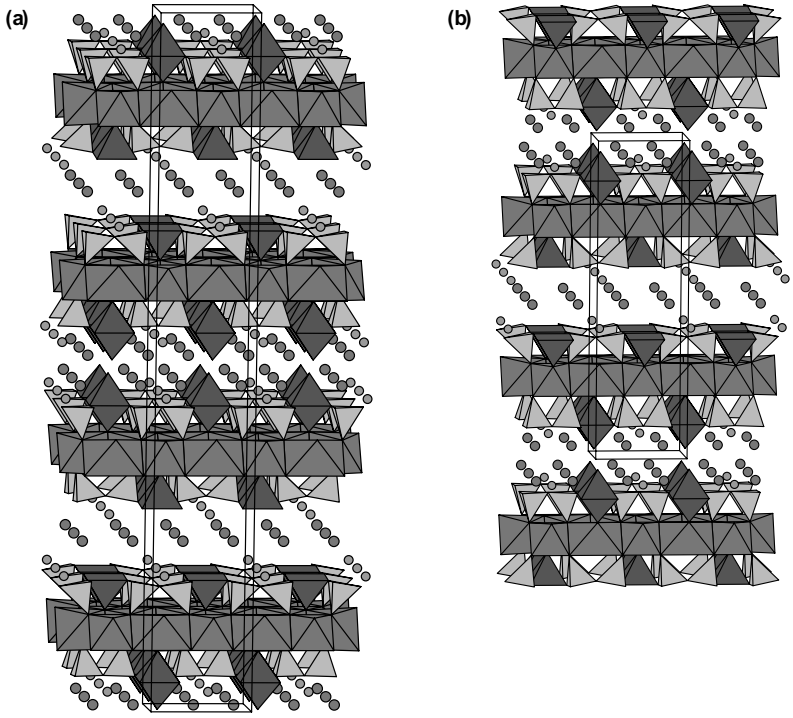

Figure 7. View along [100] of the crystal structure of two M73 polytypes. Smaller and larger circles represent cations and H_2O molecules, respectively. Note that the *X* cation shows either octahedral or pyramidal coordination (dark grey polyhedra).

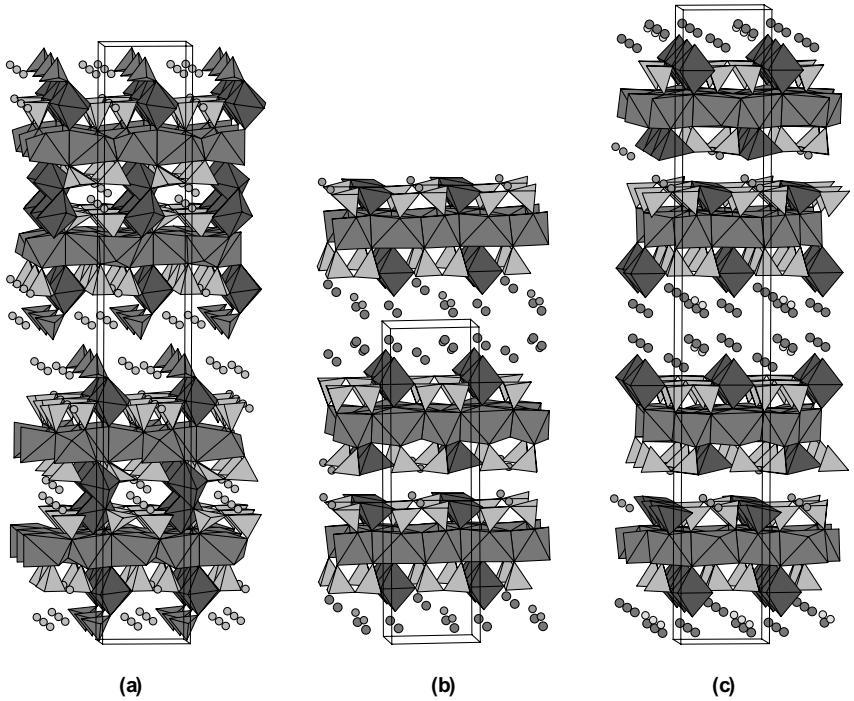

Figure 8. View along [100] of the crystal structure of bornemanite (a) and two polytypes of M72 (b and c). Circles and *X* cation as in Figure 7; dark-grey tetrahedra as in Figure 6.

(Khomyakov et al. 1992) and sobolevite (Sokolova et al. 1988). Besides nacaphite, other stoichiometric compositions may correspond to interlayer contents: $BaSO_4$ in innelite (Chernov et al. 1971); Na_3PO_4 in lomonosovite (Belov et al. 1978), vuonnemite (Ercit et al. 1998) and bornemanite (Ferraris et al. 2001a); Na_3VO_4 in $Na_8\{(NaTi)_2[Ti_2O_2Si_4O_{14}]O_2\}(VO_4)_2$ (Massa et al. 2000).

The interlayer content determines the value of the *c* parameter, which necessarily increases with the complexity of the sandwiched module (Table 2). On its own, the thickness of the *HOH* layer is about 10 Å from apex to apex of the *X* coordination polyhedra belonging to two facing *H* sheets. In the structures where the interlayer is simple, the *c* parameter is close to $n \times 10$ Å, with *n* indicating the number of *HOH* layers in the cell. Typical separations between the bases of the Si tetrahedra belonging to two facing layers are 4.2 Å in bafertisite, about 8 Å in lomonosovite and vuonnemite, 13.5 Å in quadruphite and sobolevite. However, in the minerals with the larger separation, the interlayer, besides cations, contains also complex anions even if, on the whole, behaves as a complex cation.

In some cases, more than one type of interlayer occurs in the same member of the bafertisite series. That happens in bornemanite (Fig. 8; $a = 5.498$, $b = 7.120$, $c = 47.95$ Å, $\gamma = 88.4°$, *I*11*b*; Ferraris et al. 2001a) and the two related minerals labeled M72 and M73 in Khomyakov (1995). By transmission electron microscopy (TEM), Nèmeth (2004) and Nèmeth et al. (2004a) have found two polytypes for both the latter two minerals and modeled their structures (Figs. 7 and 8). The following crystal data have been obtained by electron diffraction and refined from powder diffraction data:

M72: a = 5.552, b = 7.179, c = 25.47 Å, γ = 91.10°, $P11m$; a = 5.552, b = 7.179, c = 50.94 Å, γ = 91.10°, $I11m$.

M73: a = 5.40, b = 6.88, c = 24.01 Å, β = 91.3°, $P2/m$; a = 5.40, b = 6.88, c = 48.02 Å, β = 91.3°, $A2/m$.

The structure of bornemanite can be described as a [001] stack of $(HOH)_B$ layers: a lomonosovite-like content alternates with a seidozerite-like one[5]. A similar situation with two different interlayer contents occurs in the structures of M72 and M73 that shall be further discussed later.

In some members [bornemanite (in part; Fig. 8), perraultite, surkhobite (Fig. 6), and likely jinshajiangite (see footnote *p* in Table 2)] of the bafertisite series the layers are locked together by sharing an oxygen atom between two *X* octahedra belonging to adjacent layers. Thus, even if the *HOH* layer remains an outstanding feature of the structure, these members of the series with locked layers become framework heterosilicates and the interlayer space is divided in [100] channels with a small window like those observed in astrophyllite and nafertisite. The height of these windows corresponds to the separation between the bases of the Si tetrahedra mentioned above. Likely the "framework" members form in a later stage during the evolution of the hyperalkaline massifs; in fact, Pekov and Chukanov (2005) describe epitactic crystals with composition jinshajiangite-perraultite overgrowing true layer members with composition bafertisite-hejtmanite. These authors note that in the hyperalkaline complexes early pegmatitic titanosilicates show mainly chain- and layer-based structures, which are replaced by framework phases at a later hydrothermal stage.

Pseudosymmetries. Most of the compounds in Table 2 are either monoclinic or triclinic. As noted by Ferraris and Nèmeth (2003) and further discussed by Ferraris et al. (2004), often the values of the third periodicity and β angle are such that $c\sin(\beta - 90) \sim a/n$ (n = 3, 4, ...) holds. This relation implies that a [uvw] row with periodicity $c_o = nc\sin\beta$ and normal to the ab plane does exist. The supercell with parameters a, b and c_o is (pseudo)orthorhombic if α = 90° (monoclinic members) and (pseudo)monoclinic (angle $\alpha_m \neq 90°$) in the triclinic members with γ ~ 90°.

The occurrence of supercells favors twinning (Ferraris et al. 2004); besides, if the same supercell is shared by different members of the series, phenomena of syntactic intergrowth can occur, as reported by Nèmeth et al. (2005) for vuonnemite + epistolite + shkatulkalite and lomonosovite + murmanite. Note that, as described by Khomyakov (1995) and Pekov and Chukanov (2005), epitactic overgrowths are widespread among the minerals of Table 2, being favored by the common periodicities of their *HOH* layers.

Syntaxy and likely twinning are a main source of problems in solving and, at least, properly refining the structures of members of the bafertisite series, as discussed by Nèmeth et al. (2005) for epistolite and murmanite. In particular, these authors within a matrix of epistolite (a = 5.455, b = 7.16, c = 12.14 Å, α = 104.01, β = 95.89, γ = 90.03°) have observed syntaxy of murmanite (a =5.387, b = 7.079, c = 11.74 Å, α = 93.80, β = 97.93, γ = 90.00°) and shkatulkalite (a = 5.468, b = 7.18, c = 31.1 Å, β = 94.0°). The following closely related supercells favor the syntaxy. Epistolite: a = 5.455, b = 7.160, c = 93.728 Å, α = 88.75, β = 90.57, γ = 90.03°; murmanite: a = 5.387, b = 7.079, c = 92.843 Å, α = 89.47, β = 91.35, γ = 90.01°; shkatulkalite: a = 5.468, b = 7.18, c = 93.079 Å, α = 90, β = 90.64, γ = 90°.

An interesting case of intergrowth has been reported by Rastsvetaeva et al. (1991) for a sample of hejtmanite (Table 2), a species defined later by Vrána et al. (1992) with cell parameters

[5] Ferraris et al. (2001b), followed by Ferraris et al. (2004), called seidozerite-like the module of bornemanite with a seidozerite-like interlayer content. Note, instead, that in this module the topology of the *HOH* layer is that of $(HOH)_B$ and not of $(HOH)_V$ as in seidozerite (see also footnote 8).

(*a* and *c* exchanged): $a = 10.698$, $b = 13.768$, $c = 11.748$ Å, $\beta = 112.27°$. Rastsvetaeva et al. (1991) suggested that Sokolova et al. (1989b) failed in properly solving the structure of hejtmanite because the "single crystals" consisted of a syntaxy between two phases differing in their structures mainly for the position of Ba and the doubling of the *a* and *b* parameters. To justify the syntaxy Rastsvetaeva et al. (1991) used the following non-reduced cells: Phase (I) $P2_1/m$, $a = 5.361$, $b = 6.906$, $c = 12.556$ Å, $\beta = 119.8°$ (the corresponding reduced cell is obtained by the transformation 100/010/101: $a = 5.361$, $b = 6.906$, $c = 10.931$ Å, $\beta = 94.61°$); Phase (II) *Cm*, $a = 10.723$, $b = 13.812$, $c = 12.563$ Å, $\beta = 119.9°$ [the corresponding reduced cell used by Vrána et al. (1992) is obtained by the transformation $100/0\bar{1}0/\bar{1}0\bar{1}$].

The same type of syntaxy described for hejtmanite likely occurs also in bafertisite, the Fe-equivalent of hejtmanite, whose crystal structure has been approximately solved both in space group $P2_1/m$ ($a = 5.36$, $b = 6.80$, $c = 10.98$ Å, $\beta = 94°$; Pen and Shen 1963) and *Cm* ($a = 10.60$, $b = 13.64$, $c = 12.47$ Å, $\beta = 119.5°$; the reduced cell obtained by $\bar{1}00/0\bar{1}0/101$ is $a = 10.60$, $b = 13.64$, $c = 11.73$ Å, $\beta = 112.3°$; Guan et al. 1963). On the basis of a single-crystal diffraction pattern Yang et al. (1999) proposed that the cells of bafertisite $P2_1/m$ (Pen and Shen 1963) and *Cm* (Guan et al. 1963) correspond to a sub and true cell, respectively. The intergrowth of two phases proposed by Rastsvetaeva et al. (1991) is supported by the impossibility of properly refining the crystal structures of bafertisite and hejtmanite even in the supposed "true" cell (space group *Cm*). In fact, according to the hypothesis of the intergrowth, a proper refinement is hindered in this cell because a part of the measured reflections are contributed by different intergrown individuals.

Porous features in heterophyllosilicates

As shown above, the crystal structures of the members of the bafertisite mero-plesiotype series are based on the alternating stacking of a *HOH* layer with an interlayer module, a situation to be compared with that occurring in the 2:1 phyllosilicates. The swelling capacity of the layer silicates, normally via adsorption of H_2O molecules, depends mainly from the negative charge of the *TOT* layer. If the charge is zero (talc, pyrophyllite) or higher than about 0.6 (vermiculites, micas), swelling is not possible or can be obtained only by special procedures; smectites (e.g., montmorillonite, saponite), which have a low (0.25–0.60) charge, typically swell. The capacity to swell of the smectites is the property that promotes the use of these clay minerals to prepare pillared clays (cf. Cool et al. 2002).

Pillaring. According to the IUPAC nomenclature (Schoonheydt et al. 1999), "pillaring is the process by which a layered compound is transformed into a thermally stable micro- and/or mesoporous material with retention of the layer structure. A pillared derivative is distinguished from an ordinary intercalate by virtue of intracrystalline porosity made possible by the lateral separation of the intercalated guest." A pillared material differs from an ordered porous material by having disordered channels. In fact, whereas pillared materials have periodically stacked layers, let say along [001], and their diffraction patterns show sharp 00*l* maxima, the interlayer pillared content is not stacked coherently.

The process of pillaring of a layered material includes the following steps (Fig. 9) whose details are not yet completely understood (Cool et al. 2002): swelling in a polar solvent (usually water); substitution of the original interlayer cations by bulky (inorganic/organic) cations (pillaring agent); washing (further chemical reactions occur at this step); calcination (pillars are formed).

Pillaring materials (e.g., pillared clays) show the following basic characteristics.

- The interlayer spacing increases from the original value of ~ 5 Å to at least ~15 Å.
- The layers do not collapse under calcination.

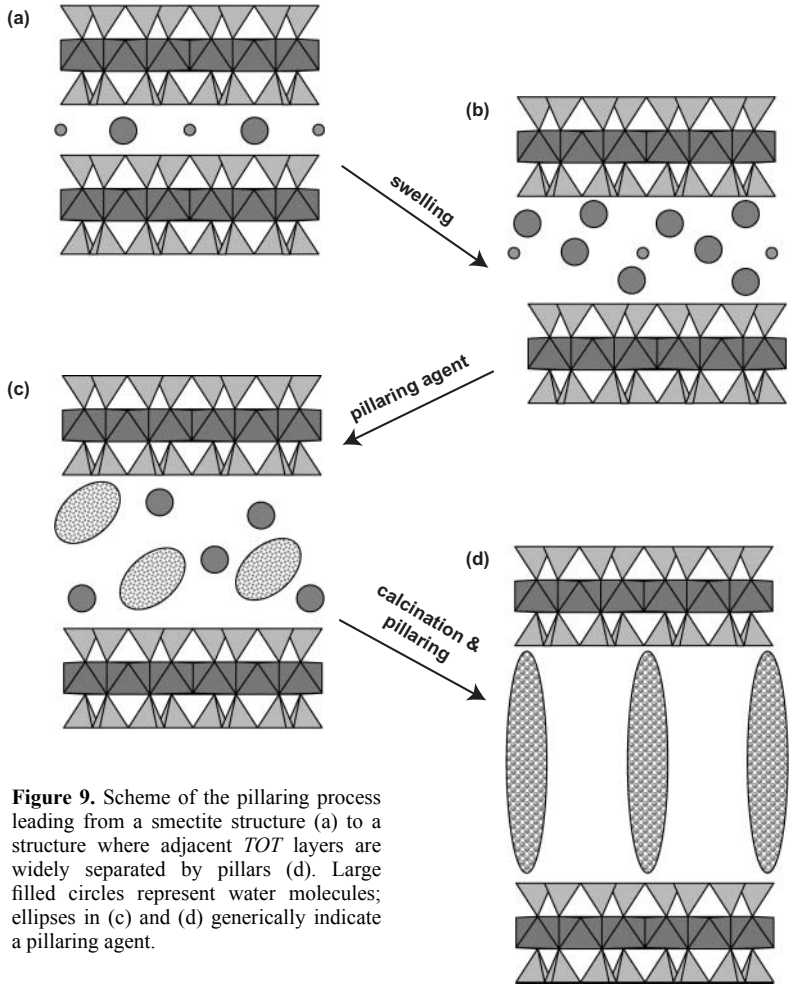

Figure 9. Scheme of the pillaring process leading from a smectite structure (a) to a structure where adjacent *TOT* layers are widely separated by pillars (d). Large filled circles represent water molecules; ellipses in (c) and (d) generically indicate a pillaring agent.

- The pillaring agent (inorganic/organic) is laterally spaced.
- The interlayer space is porous: at least N_2 molecules can go through, namely the pore has a window of about 3.2 Å.
- Not necessarily, pores and pillars are ordered; in fact, in a pillared material usually only the 00*l* reflections are sharp.

Leaching and solid state transformations[6]

As documented in this volume by Chukanov and Pekov (2005) and Pekov and Chukanov (2005), leaching of cations in natural conditions is quite common for the microporous

[6] Note that the wording "solid-state transformation" widely used in this chapter does not exclude the intervention of local dissolution and re-crystallization processes. "Solid state transformation" intends to emphasize that primary and secondary phases differ mainly for the interlayer contents in a way that, at least formally, is amenable to leaching/exchange processes. On the other side, the real nature of the processes of mineral substitutions in "solid state" at atomic level is currently matter of debate (cf. Putnis 2002).

framework heterosilicates that often occur with the heterophyllosilicates. As we shall see in this section, the phenomenon is documented also for the latter minerals. The mentioned authors affirm that ion exchange with the circulating solutions, during the post-crystallization steps in the course of the evolution of the hyperalkaline massifs, is the easiest way to adequate the stability of the crystal structure to the changing geological conditions (see also the Section "Transformation Minerals" below).

In a layered structure like those of the heterophyllosilicates of Table 2, deficiency of interlayer cations, in particular Na^+, can be expected and is not uncommon even in micas[7]. Such deficiency not necessarily is due to leaching; it can be there since the original crystallization process. A later loss of cations (decationization) by leaching must involve a re-adjustment in the structure and requires some exchange capacity with the surrounding medium. Whereas in phyllosilicates the non-tetrahedral cations of the *TOT* layer are tightly locked within the octahedral *O* sheet and typical leachable cations, like Na^+, are normally absent there (but see the recently described mica shirokshinite containing octahedral Na; Pekov et al. 2003), in the heterophyllosilicates the presence of Na^+ in the *O* sheet is common. Because of its large ionic radius, the introduction of this cation leads usually to some deformation of the *O* sheet, a feature that may favor leaching as exemplified below by delindeite.

Delindeite. The structure of delindeite (Fig. 10) offers an example of a solid-state modification involving leaching of Na from the *O* sheet. Ferraris et al. (2001b) proved that an Na deficiency affects sites in the *O* sheet of the *HOH* layer in delindeite (Table 2; $a = 5.327$, $b = 6.856$, $c = 21.51$ Å, $\beta = 93.80°$, $A2/m$), a quite unusual situation for a layer structure where the more weakly bonded cations reside in the interlayer. Unlike most compounds of Table 2, where the *O* sheet is occupied by typical octahedral cations as Fe, Mn and Mg, two independent Na sites occur in the *O* sheet of delindeite. One Na atom incorporates in its large and disordered coordination sphere also a bridging Si-O-Si oxygen atom that, in heterophyllosilicates, normally belongs to the *H* sheet only. In other words, in delindeite a basal oxygen atom of a silicon tetrahedron is captured within the large coordination sphere of Na. Thus, the Na^+ cation "sees" directly the interlayer space through a window of the *H* sheet and some exchange with the surrounding medium becomes feasible. A statistical distribution of the captured oxygen on two independent positions avoids the strain of an O···O edge shared between *H* and *O* sheets.

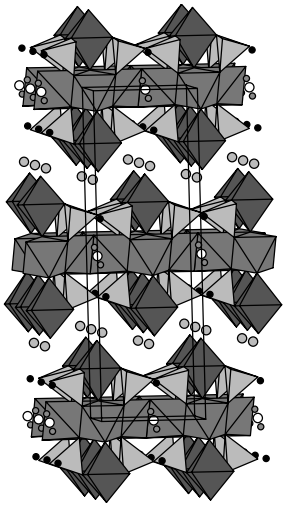

Figure 10. View along [100] of the crystal structure of delindeite. The black circles represent the disordered bridging oxygen atom that is within the coordination sphere of a Na^+ cation (blank circles) belonging to the *O* sheet (see text). Grey circles represent interlayer cations.

A similar coordination to a bridging oxygen atom belonging to the *H* sheet has been reported in the structure of seidozerite (Pushcharovsky et al. 2002)[8]

[7] A murmanite-related phase that is almost devoid of interlayer content has been found in Lovozero massif by N.V. Chukanov (personal communication).

[8] The inclusion of a bridging oxygen atom within the coordination sphere of Na belonging to the *O* sheet introduces a further peculiarity in the *HOH* layer of seidozerite. Consequently, contrary to what reported in previous literature, in this chapter statements like "seidozerite derivatives" or "seidozerite-like *HOH* layer" for the heterophyllosilicates of Table 2 are avoided (see also footnotes 5 in the text and *g* in Table 2).]

and can be compared with situations found in members of the rhodesite group described below. Na^+ vacancies in the *O* sheet require a charge balance that is provided by the $O^{2-} \rightarrow OH$ substitution, like in steenstrupine-(Ce) (Makovicky and Karup-Møller 1981).

Transformation minerals. There are consistent evidences of solid-state transformation from one to another member of Table 2 via leaching/substitution of the interlayer composition. In some cases, swelling processes become evident by comparing the structures of the parent and daughter phases (see below). As summarized by Khomyakov (1995) on the basis of his previous work (cf. also Chukanov and Pekov 2005 and Pekov and Chukanov 2005), an active interaction with water is a characteristic of many highly alkaline titanosilicates like the heterophyllosilicates of Table 2. Several stage-by-stage replacements of anhydrous titanosilicates by their hydrated and decationated analogues are described in the quoted literature, including the following two reactions that are of interest in this chapter: lomonosovite + $H_2O \rightarrow$ murmanite + Na_3PO_4; vuonnemite + $H_2O \rightarrow$ epistolite + Na_3PO_4 (+shkatulkalite?).

Often the transformation is topotactic as witnessed by the occurrence of oriented intergrowths and pseudomorphs after the parent phase. Based on electron and X-ray diffraction studies, intergrowths of epistolite and shkatulkalite (transformation phases) with murmanite (primary phase) are reported by Nèmeth et al. (2005); Sokolova and Hawthorne (2001) report intergrowths of lomonosovite (primary phase) with the transformation phases quadruphite, polyphite and sobolevite, all containing PO_4 groups that share a corner with the octahedron of the *X* cation (Table 2). Pekov and Chukanov (2005) report the following pseudomorphs of framework heterosilicates after members of the bafertisite series: labuntsovite-group minerals after lomonosovite, vuonnemite, astrophyllite and lamprophyllite; zorite and Na-komarovite after vuonnemite; sitinatikite and narsarsukite after lomonosovite; vinogradovite and kukisvumite after lamprophyllite. According to Khomyakov (1995), the new phases, that have been called transformation minerals, can be formed only by transforming primary minerals that instead crystallize from melts or fluids.

Khomyakov (1995) wrote that for some phases the transformation is active at atmospheric conditions ("Under natural atmospheric conditions anhydrous peralkaline titanosilicates undergo a spontaneous transition to their low-alkaline hydrogen-bearing analogues. This transition may be described as a reaction between the sodium-supersaturated solid phase and the atmospheric water."). Other phases, as it happens for the mentioned transformations of lomonosovite and vuonnemite, "which are stable under atmospheric conditions, are readily hydrated in the epithermal and hypergene processes."

Following Khomyakov's suggestion (cf. Khomyakov 1995), in Russian literature, the often-observed preservation of structure modules through the transformation from primary to secondary phases (usually via a topotactic reaction) is known as *inheritance principle*; the minerals involved in the steps of a transformation are said to form an *evolutionary series*, a concept useful in understanding the mineral associations and the geological evolution of the hyperalkaline formations (cf. Pekov and Chukanov 2005). For example, in the Ilímaussaq peralkaline massif the secondary phases epistolite and murmanite have been first discovered; only later, following the hypothesis on transformations reported above, the corresponding primary phases vuonnemite and lomonosovite have been identified.

Transformation minerals after vuonnemite and lomonosovite. Vuonnemite (Fig. 6) and lomonosovite (Fig. 11; Table 2) are primary (parent) minerals that, as written above, by leaching of their PO_4 groups and hydration transform into secondary (daughter) phases (Figs. 11 and 12). The solid-state nature of these transformations (but see footnote 6) is supported by abundant findings of pseudomorphs of the secondary phases after the primary ones and a wide occurrence of oriented intergrowths between them, as recently proved

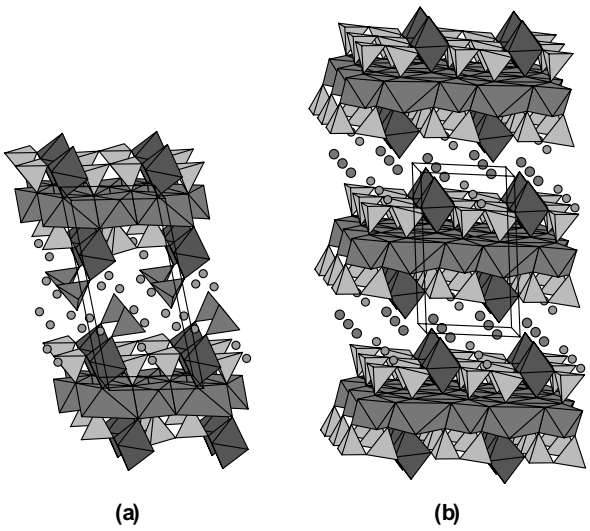

Figure 11. View along [100] of the crystal structure of the primary phase lomonosovite (a) that is transformed into the secondary phase murmanite (b) via leaching of PO_4 groups (dark grey tetrahedra) and hydration. Circles as in Figure 7.

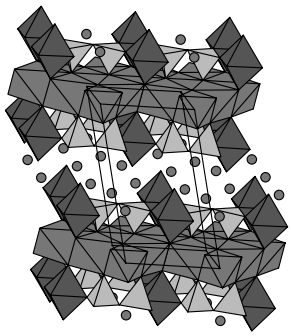

Figure 12. View along [100] of the crystal structure of epistolite, a secondary phases derived from vuonnemite (Fig. 6b) via leaching of PO_4 groups and hydration (large grey circles).

by electron and single-crystal X-ray diffraction studies (Nèmeth et al. 2005). Note that the occurrence of intergrowths involving primary and secondary phases and, if the case, other phases is considered a main source of difficulties in properly solving and refining the corresponding structures [cf. vuonnemite + epistolite + shkatulkalite in Nèmeth et al. (2005)]. Because of the loosing of PO_4, the width of the interlayer is smaller in the secondary phases, but the swelling contribution of hydration is evident.

Transformation minerals after bornemanite. Khomyakov (1995) reported that the mineral labeled M72 is pseudomorph after bornemanite (Table 2). Khomyakov (2004) showed that bornemanite exchange $Na_3(PO_4)$ for H_2O when treated with boiling water.

As mentioned above, by electron (SAED) and X-ray (powder) diffraction, Nèmeth et al. (2004a) have shown that M72 consists of two polytypes and modeled their structures (Fig. 8). The swelling action of the transformation is evident in the separation of the two *X* octahedra, which in bornemanite share an edge, and by the overall increase of the *c* parameter (Table 2) in spite of the fact that PO_4 groups are leached.

A similar transformation is observed for M73 (Nèmeth 2004); the parent phase of M73 is not exactly identified but likely is a bornemanite-type phase. Again, two polytypes have been identified and their structure modeled. The two polytypes of M73 differ from those of M72 mainly for a different arrangement of the two interlayer contents (Fig. 7). The *X* cation is present with coordination numbers 5 and 6 both in M72 and M73. Interesting to note that, contrary to M72, M73 shows the widest interlayer between two *H* sheets with *X* in coordination 5.

Note that in some cases the coordination number of the *X* cation decreases from six in the parent phase to five in the daughter phase (Figs. 8, 12). That may be related either to the removal of PO_4 groups that share an oxygen atom with the *X* cation, or to the separation of *X* octahedra that were locked together in the primary phase.

Pillared derivatives?

We have mentioned that the *TOT* layers of smectites, which bear an intermediate negative charge, are the best starting material to prepare pillared clays because of their easy swelling, a property observed in nature and exploited in laboratory. Above it has been shown that processes able to modify the interlayer content of the heterophyllosilicates via solid-state reactions are active in nature. In particular, as recently discussed by Ferraris (2004) and Nèmeth et al. (2004b), the secondary phases that are formed via the following transformation seem to be suitable candidates for investigating swelling properties in view of preparing pillared materials based on *HOH* layers: vuonnemite → epistolite (plus shkatulkalite?); lomonosovite → murmanite plus an unidentified phase reported by Semenov et al. (1962); bornemanite → M72; bornemanite-type → M73.

So far, there is no record in the literature of the use of heterophyllosilicates for obtaining pillaring porous materials. Even the knowledge on the exchange capacity of these minerals leading to secondary phases is acquired mainly from field observations, being experimental investigation still scarce (but see Chelishchev 1972).

Reasons of the limited experimental investigation can be a limited knowledge of the heterophyllosilicates among materials scientists, and difficulties in synthesizing these compounds; a step, this one, which for sure is needed because the minerals listed in Table 2 are generally rare and show a complex chemical composition. The only *ab initio* synthetic bafertisite-type compound reported in the literature is an anhydrous vanadate, $Na_8\{(Na,Ti)_4[Ti_2O_2Si_4O_{14}]O_2\}(VO_4)_2$, that corresponds to the phosphate lomonosovite and has been prepared by crystallization from a melt (Massa et al. 2000). It can be mentioned also that by heating a mixture of natural lamprophyllite and nepheline at about 900°C, Zaitsev et al. (2004) have obtained new formed lamprophyllite with a composition different from that of the starting sample. However, by analogy with the 2:1 phyllosilicate smectites, one may conclude that the hydrated phases of heterophyllosilicates look as the best candidates to attempt swelling in these titanosilicates.

According to Khomyakov (1995) (cf. Pekov and Chukanov 2005), the secondary hydrated phases of heterophyllosilicates are likely to be obtained only via solid-state transformation, for sure an obstacle towards synthesis. An alternative is finding conditions to swell directly primary anhydrous phases as it has been possible with micas (cf. Cool et al. 2002). Recently, Ustinov and Ul'yanov (1999) have obtained murmanite by hydrothermal transformation of lomonosovite at 100°C. Khomyakov (2004) obtained murmanite and epistolite from, in the order, lomonosovite and vuonnemite treated with boiling water; as mentioned above, under the same conditions he showed also that "beta-lomonosovite" and bornemanite exchange $Na_3(PO_4)$ and Na for H_2O.

Some inspiration on the synthesis of the secondary hydrated phases of heterophyllosilicates might be found in the variety of methods utilized for the synthesis of smectites (cf. Güven 1988).

PALYSEPIOLES

Sepiolite, palygorskite and related structures

Sepiolite, ideally $Mg_8[Si_{12}O_{30}](OH)_4 \cdot 12H_2O$, and palygorskite (also known as attapulgite), ideally $Mg_5[Si_8O_{20}](OH)_2 \cdot 8H_2O$, are important clay minerals. Their crystal structures are known only through powder diffraction data. Sepiolite is orthorhombic, *Pncn*, with cell parameters a = 13.40, b = 26.80, c = 5.28 Å (Brauner and Preisinger 1956). For palygorskite

two polytypes are known (Artioli and Galli 1994); Chiari et al. (2003) report the following crystal data for the two polytypes: *C2/m*, $a = 13.337$, $b = 17.879$, $c = 5.264$ Å, $\beta = 105.27°$; *Pbmn*, $a = 12.672$, $b = 17.875$, $c = 5.236$ Å.

The structures of sepiolite and palygorskite are based on a framework of chessboard connected *TOT* ribbons. These ribbons develop along [001] and correspond to cuts with different width of a phyllosilicate 2:1 layer; they delimit [001] channels (Fig. 13). In the [010] direction, the $(TOT)_S$ ribbon of sepiolite is one chain wider than that, $(TOT)_P$, of palygorskite. This feature requires for sepiolite a *b* value about 9 Å longer than that of palygorskite, i.e., about 4.5 Å per added *T* chain. The minimum effective width of the channel windows in palygorskite and sepiolite is the same (about 4.5 Å). The frameworks of sepiolite and palygorskite can be seen also as modulated *TOT* silicate layers showing a waving *T* sheet and a discontinuous *O* sheet (Guggenheim and Eggleton 1988).

By refinement carried out with neutron-diffraction data collected on a deuterated powder sample of palygorskite, Giustetto and Chiari (2004) showed that only highly disordered zeolitic H_2O is present in the channels of the structure. The same evidence is obtained by ^1H NMR investigation on dehydrated and rehydrated palygorskite (Kuang et al. 2004). Based on a critical review of compositional data available in literature, Galan and Carretero (1999) proved that whereas sepiolite is a true trioctahedral mineral, palygorskite is intermediate between di- and trioctahedral composition because some trivalent cations (e.g., Al) always occur in the octahedral sites. The intermediate di- trioctahedral character of palygorskite is confirmed by IR spectroscopy (Chahi et al. 2002). A recent IR investigation (García Romero et al. 2004) reveals absence of trioctahedral Mg in the Mg-richest (3.11 apfu) sample of palygorskite so far known.

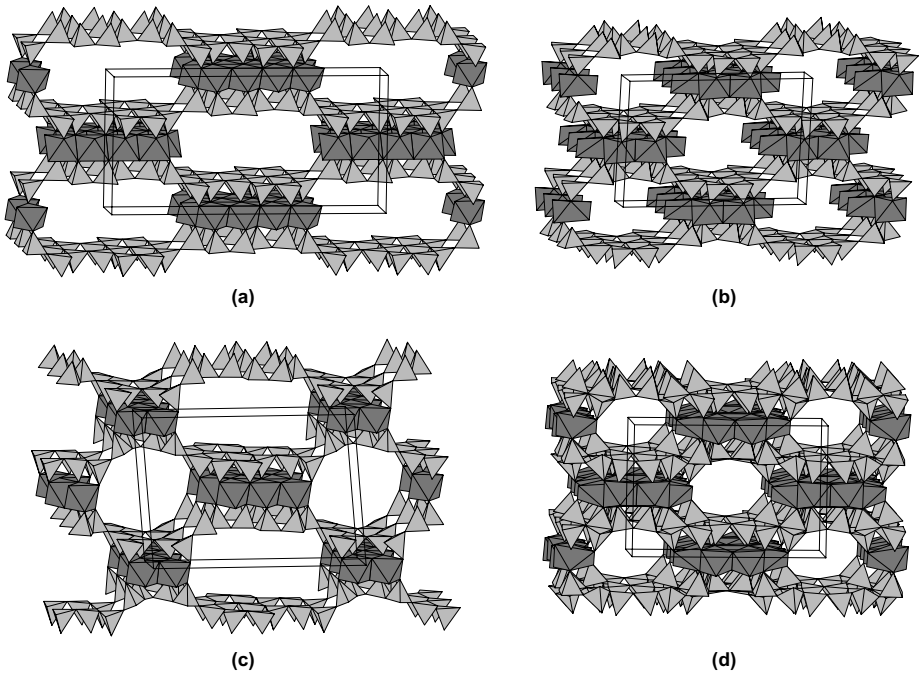

Figure 13. View along [001] of the crystal structure of sepiolite (a), palygorskite (b), kalifersite (c) and intersilite (d); *a* vertical axis. The content of the [001] channels is not drawn.

Kalifersite – a hybrid between sepiolite and palygorskite. Kalifersite, $(K,Na)_5(Fe^{3+})_7[Si_{20}O_{50}](OH)_6 \cdot 12H_2O$, is a rare [001] fibrous silicate found in a hydrothermally altered pegmatite at Mt. Kukisvumchorr (Khibina alkaline massif, Kola Peninsula, Russia). It is triclinic (a = 14.86, b = 20.54, c = 5.29 Å, α = 95.6, β = 92.3, γ = 94.4°, $P\bar{1}$); Ferraris et al. (1998) succeeded to model its crystal structure (Fig. 13) after realizing a modular relationship with sepiolite and palygorskite as follows.

(i) Kalifersite, sepiolite and palygorskite have close values of their a and c parameters; the latter corresponds to the fibrous direction of these silicates and to the periodicity of a pyroxene chain.

(ii) The b value of kalifersite is intermediate between that of palygorskite and sepiolite.

(iii) The $[Si_{20}O_{50}](OH)_6$ silicate anion of kalifersite corresponds to the sum of those of sepiolite, $[Si_{12}O_{30}](OH)_4$, and palygorskite, $[Si_8O_{20}](OH)_2$.

(iv) Martin-Vivaldi and Linares-Gonzales (1962) have interpreted X-ray powder diffraction patterns intermediate between those of palygorskite and sepiolite as random intergrowths of $(TOT)_S$ and $(TOT)_P$ ribbons.

Taking into account the above chemical and crystallographic aspects, a structure model for kalifersite based on a 1:1 chessboard arrangement of $(TOT)_P$ and $(TOT)_S$ [001] ribbons and the filling of the channels with alkalis and water molecules was obtained (Fig. 13). Due to the longer a parameter, the minimum effective widths (~ 5.4 and ~ 6.2 Å) of the two types of channels in kalifersite are larger than the corresponding ones in palygorskite and sepiolite (~ 4.5 Å).

The polysomatic series of palysepioles. Palygorskite (*P*), and sepiolite (*S*) are the end members of the *palysepiole* (*paly*gorskite + *sepiol*ite) polysomatic series P_pS_s defined by Ferraris et al. (1998); kalifersite is the P_1S_1 member. Falcondoite (Springer 1976) and loughlinite (Fahey et al. 1960) differ from sepiolite only in the composition of the octahedral part; the same situation is valid for yofortierite (Perrault et al. 1975) and tuperssuatsiaite (Cámara et al. 2002) in comparison to palygorskite. Chukanova et al. (2002) have described an orthorhombic unnamed mineral from Mt. Flora (Lovozero massif) with composition $(Fe,Mn)_4Si_6O_{15}(OH)_2 \cdot nH_2O$ and cell parameters a = 13.53, b = 26.70, c = 5.13 Å; it corresponds to a Fe-dominant sepiolite.

Merotypes and plesiotypes of palysepioles

Raite – a structure based on a palygorskite framework. The titanosilicate raite, $Na_3Mn_3Ti_{0.25}[Si_8O_{20}](OH)_2 \cdot 10H_2O$, is a rare silicate found in the Yubileinaya pegmatite at Mt. Karnasurt (Lovozero alkaline massif, Kola Peninsula, Russia). Raite is monoclinic (*C2/m*, a = 15.1, b = 17.6, c = 5.290 Å, β = 100.5°; Pushcharovsky et al. 1999) and its crystal structure consists of a palygorskite-like framework, but the channel content differs substantially from that of palygorskite both in chemistry and structure. Practically, in raite the *O* sheet is not interrupted even if a part of the octahedra that reside in the channels are 3/4 vacant and only 1/4 occupied by Ti. Thus, raite and palygorskite share only the *TOT* building module and are therefore in merotypic relationship.

Intersilite. This rare titanosilicate occurs at Mt. Alluaiv (Lovozero alkaline massif, Kola Peninsula, Russia) and has chemical composition $(Na,K)Mn(Ti,Nb)Na_5(O,OH)(OH)_2[Si_{10}O_{23}(O,OH)_2] \cdot 4H_2O$. In its structure ($a$ = 13.033, b = 18.717, c = 12.264 Å, β = 99.62°, *I2/m*; Yamnova et al. 1996), sepiolite-like ribbons partially overlap along [010] because of tetrahedral inversions within the same ribbon (Fig. 13). Due to the substantial modification of the sepiolite framework, intersilite is in plesiotype relationship with the palysepiole polysomatic series. The minimum effective width of the channels is ~ 3.5 Å.

Microporous features of palysepioles

Modern chemical (Galan and Carretero 1999) and structural (Giustetto and Chiari 2004) analyses prove that only H_2O molecules reside in the structural channels of the clay minerals sepiolite and palygorskite. The recent finding of kalifersite and raite shows that in nature, under appropriate conditions, the channels of sepiolite- and palygorskite-like frameworks can be almost fully filled with M^{n+} cations (n =1 to 4), including Ti; in these structures the "octahedral" *O* sheet is no longer discontinuous. The occurrence of Ti in raite realizes a bridge between palysepioles and titanosilicates.

In nature, interactions at nanoscale between the clay minerals palygorskite and sepiolite and the surrounding medium are well known, even if not always it is clear if they are related to adsorption via the wide free surface of the particles, to absorption in the interlayer or to both mechanisms (cf. Velde 1992). This is the case, for example, of the adsorption of humic acid by palygorskite and sepiolite (Singer and Huang 1989) and the curious association of quinone pigments with Eocene sepiolite known as quincyte (Louis et al. 1968; Prowse et al. 1991).

Pre-tech era applications. As summarized by Chiari et al. (2003) in the introduction of their paper on the interaction between the host palygorskite framework and the guest indigo, Maya Blue is a characteristic pigment produced by the Mayas around the VIII century AD; its color ranges from a bright turquoise to a dark greenish blue. It has been shown that the pigment contains palygorskite (in some cases, minor sepiolite) and its color is due to the presence of indigo that the Mayas obtained from a vegetable. Experimentally, it has been shown that the simple technique required to prepare the pigment, namely mixing palygorskite and *Indigofera suffruticosa* then filtering after heating at about 100°C, was accessible to the Mayas.

Sepiolite has been used for hundreds of years in southern Spain for the purification of wine (Galan and Ferrero 1982).

Modern technological applications. The exploitation of the capacity of palygorskite and sepiolite to absorb organic molecules already known to Mayas is a wide practice in modern technology. However, not always the structural channels are the only sites active in sorption, surface mechanisms being active (cf. Shariatmadari et al. 1999). To the list of applications reviewed by Jones and Galan (1988) and Galan (1996), only some quotations of recent results are here added. These include: sorption of heavy metals from industrial waste water (cf. Garcia Sanchez et al. 1999); removal of dyes from tannery waste waters (cf. Espantaléon et al. 2003); stabilization of dyes and pesticides (cf. Casal et al. 2001; Rytwo et al. 2002); template synthesis of carbon nanofibers (Fernandez-Saavedra et al. 2004); preparation of Ni and Pd catalysts (Anderson and Galan-Fereres 1999; Corma et al. 2004).

Future directions of research. No technological uses are known for the other palysepioles and related structures mentioned above. Actually, all of them are rare minerals and have been discovered only recently. To test their properties it would be necessary to have some quantity of synthetic material. Presumably, the synthesis is feasible by hydrothermal method as done for sepiolite (Mizutani et al. 1991).

Actually, only kalifersite is based on a guest framework substantially differing from those of both palygorskite and sepiolite. In fact, kalifersite incorporates in its structure the two types of channels that occur singly in sepiolite and palygorskite; thus, in principle, the composite silicate framework of kalifersite could display at the same time the absorption features of the two clay minerals. Other structures described in this section incorporate the high-charge cation Ti^{4+}, an element well known for its catalytic activity. Likely, palysepiole frameworks based on ribbons wider than those occurring in sepiolite could be synthesized, thus realizing pores with at least one larger dimension of the window. In fact, the bridges that connect the segments of inverted tetrahedra limit the second dimension of the window.

Some porous structures related to palysepioles

Ferraris et al. (2004) pointed out that the crystal structure of the lithium silicate silinaite ($NaLiSi_2O_5 \cdot 2H_2O$; *C*2/*c*, *a* = 14.383, *b* = 8.334, *c* = 5.061 Å, β = 96.6°; Grice 1991) shows a chessboard arrangement of narrow *TOT*-like ribbons comparable to those of palysepioles such that ten-membered channels filled by Na and H_2O are formed (Fig. 14). Whereas in palygorskite and sepiolite the inversion of the tetrahedral sheet is every four and six tetrahedra, respectively, in silinaite the same inversion is every two tetrahedra. Besides, the *O* part of the silinaite *TOT*-like ribbon consists of Li tetrahedra instead of octahedra as in palysepioles and, in general, in the phyllosilicates. The ten-membered channels are delimited by eight Si tetrahedra and two Li tetrahedra. The minimum effective width of these channels is about 5.5 Å.

Ten-membered channels (Fig. 14) occur also in lintisite [$Na_3LiTi_2(Si_2O_6)_2O_2 \cdot 2H_2O$; Merlino et al. 1990], a mineral mentioned in this volume by Chukanov and Pekov (2005) together with other titanosilicates, which Ferraris et al. (2004) reported as members of a merotype series based on three structural modules that are typical of the following phases: silinaite, lorenzenite, $Na_4Ti_4(Si_2O_6)_2O_2$, and a hypothetic *Z* zeolite, $(Na,K)Si_3AlO_8 \cdot 2H_2O$. Whereas the channels of silinaite consist of eight Si tetrahedra and two Li tetrahedra, those of lintisite have four Si tetrahedra replaced by Ti octahedra. The minimum effective width of the channels in lintisite is slightly smaller than in silinaite.

SEIDITE-(Ce) AND RELATED STRUCTURES

The silicate double layer with eight-membered channels that occurs in the crystal structure of the titanosilicate seidite-(Ce) (Fig. 15) is present also in a group of well known microporous structures reported in this volume by Rocha and Lin (2005). In this chapter we refer to the frameworks of these heterosilicates as the rhodesite-type structure; this structure type is compared with the structure of seidite-(Ce) and their modular aspects are emphasized (cf. Ferraris et al. 2004).

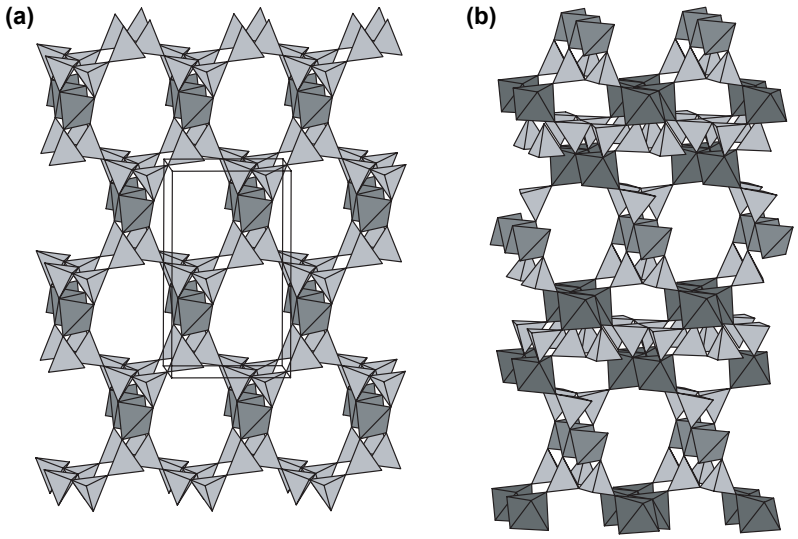

Figure 14. View of the crystal structure of silinaite, along [100] (a), and lintisite along [001] (b; *a* vertical axis). The dark grey tetrahedra are centered by Li. The content of the channels is not shown.

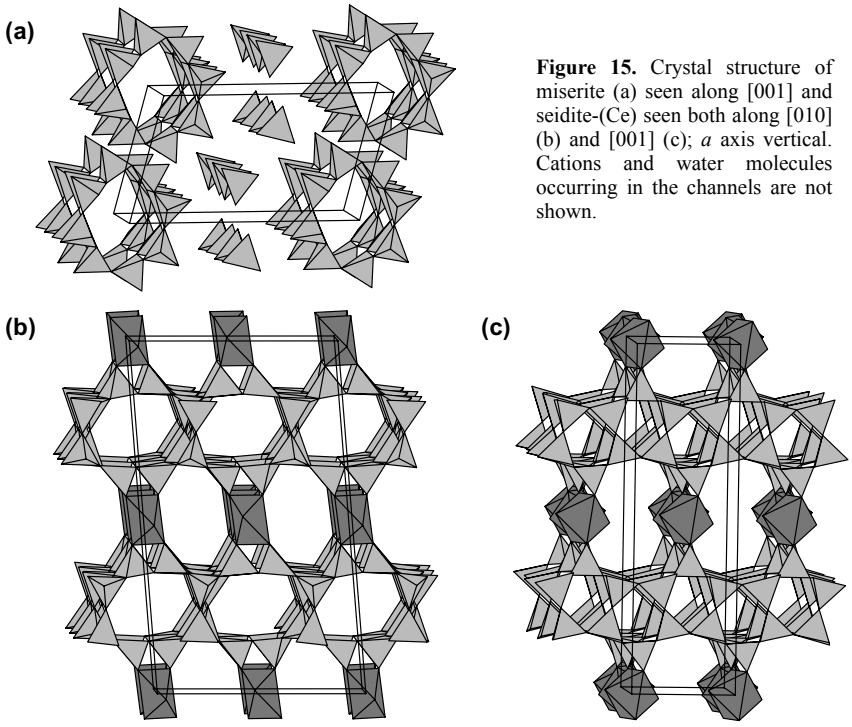

Figure 15. Crystal structure of miserite (a) seen along [001] and seidite-(Ce) seen both along [010] (b) and [001] (c); *a* axis vertical. Cations and water molecules occurring in the channels are not shown.

Modeling the structure of seidite-(Ce)

Seidite-(Ce), $Na_4(Ce,Sr)_2\{Ti(OH)_2(Si_8O_{18})\}(O,OH,F)_4{\cdot}5H_2O$, is a titanosilicate found in the Yubileynaya pegmatite at Mt. Karnasurt (Lovozero alkaline massif, Kola Peninsula, Russia) and first described by Khomyakov et al. (1998). Because of its disordered [010] fibrous morphology, single crystals suitable for X-ray crystallography are not available and its crystal structure (a = 24.61, b = 7.23, c = 14.53 Å, β = 94.6°; $C2/c$; Fig. 15) was modeled by Ferraris et al. (2003) on the basis of electron (SAED) and X-ray powder diffraction data. Even if finally the structure of seidite-(Ce) turned out to share its silicate module with rhodesite $\{K_2Ca_4[Si_8O_{18}(OH)]_2{\cdot}12H_2O$; a = 23.416, b = 6.555, c = 7.050 Å, *Pmam*; Hesse et al. 1992$\}$ and related structures (see below), Ferraris et al. (2003) have got the key for its modeling after comparison with the structure of miserite (Scott 1976). The latter structure shows microporous features (Fig. 15), being about 2.8 Å the minimum effective width of its isolated eight-membered channels.

Ferraris et al. (2003) noted that the cell parameters of miserite (*m*) [$KCa_5(Si_2O_7)(Si_6O_{15})(OH)F$; a = 10.100, b = 16.014, c = 7.377 Å, α = 96.41, β = 111.15, γ = 76.57°; $P\bar{1}$] and seidite-(Ce) (*s*) are related as follows: $a_s \cong 2a_m$, $c_s \cong b_m$, $b_s \cong c_m$. Furthermore, the oblique (010) lattice net of miserite can be described as based on a centered rectangular cell with parameters very close to those of the centered (001) net of seidite-(Ce). It was also noted that formally the same $(Si_8O_{22})^{12-}$ silicate anion occurs in both minerals; instead, the number of non-silicate cations is 6 in miserite and 7 in seidite-(Ce), the chemically most important difference being the presence of the high-charge Ti^{4+} cation in the latter mineral. By rotation of the isolated Si_2O_7 groups that alternate with [001] eight-membered silicate channels in the structure of miserite, the (100) silicate layer consisting of interconnected channels typical of seidite-(Ce) is obtained

(Fig. 15). In their turn, the (100) silicate layers are connected by isolated Ti octahedra, thus obtaining a three-dimensional mixed tetrahedral/octahedral framework.

The (100) layer of the eight-membered channels corresponds to the double silicate layer that occurs in the microporous mineral rhodesite (Hesse et al. 1992) and related compounds. A xonotlite-like [$Ca_6Si_6O_{17}(OH)_2$; *P*2/*a*, *a* = 17.032, *b* = 7.363, *c* = 7.012 Å, β = 90.36°; Hejny and Armbruster 2001] chain, i.e., a double wollastonite-like chain, delimits the (010) front windows of the double layer. As discussed below, both the upper and lower (100) walls of the silicate double layer consist of an apophyllite-type [$KCa_4(Si_8O_{20})F{\cdot}8H_2O$; *P*4/*mnc*, *a* = 8.965, *b* = 8.965, *c* = 15.768 Å; Colville et al. 1971] net that includes eight- and four-membered rings. Being the upper (100) wall staggered by *b*/2 relative to the lower wall, the window rings of the two walls are not aligned, and the [100] direction does not show pores. A second type of eight-membered channels crosses the structure of seidite-(Ce) along [010]; in these channels, two out of eight polyhedra forming the window are Ti octahedra.

A further double system of channels extends along [001] (Fig. 15). One set of channels of this system consists of ten-membered pores with two Ti octahedra as ring members; the second set corresponds to five-membered channels delimited by tetrahedra only. Each set forms alternating (100) layers. The front windows of the five-membered channels correspond to the (001) wall of the [010] eight-membered silicate channels.

The wollastonite chains that develop along [010] and [001] determine the periodicity of both sets of channels. Note that the [001] five-membered rings of seidite-(Ce) correspond to the eight-membered [010] rings in rhodesite (Fig. 16), the different cross-section being related to the *b*/2 stagger of the (100) apophyllite-type sheets mentioned above.

Microporous properties

The first experimental evidence of microporous features in seidite-(Ce) was the high value of its measured density, 3.21 g/cm^3 as determined by Clerici liquid [an aqueous solution of $CH_2(COO)_2Tl_2{\cdot}HCOOTl$] vs. the calculated value of 2.75 g/cm^3. This high value was due to absorption of Tl, as confirmed by an electron microprobe analysis of grains of the mineral

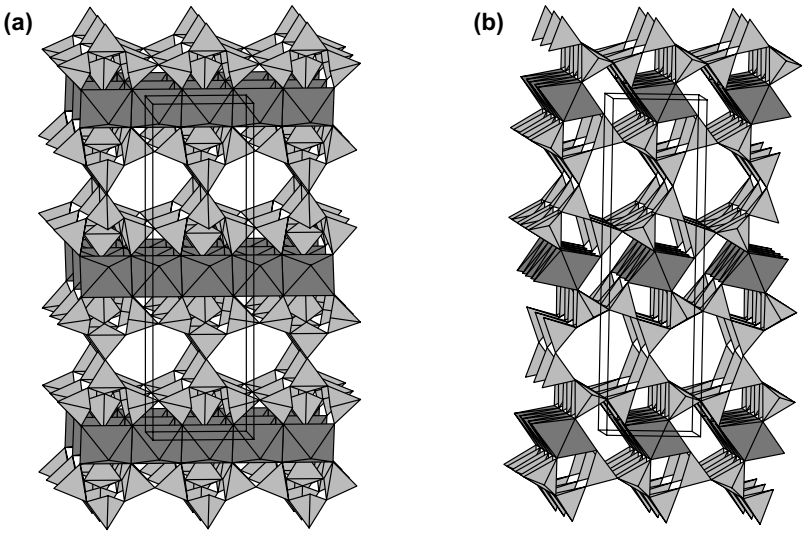

Figure 16. Crystal structure of rhodesite seen along [010] (a) and [001] (b). Cations and water molecules occurring in the channels are not shown; *a* axis vertical.

that had been kept in aqueous solution of Tl^+, K^+, Rb^+, Cs^+ and Ba^{2+} at room temperature for periods of 6–8 weeks: Na was substituted by the shown cations (Khomyakov et al. 1998).

The presence of channels in the structure and weak bonding of guest Na to the host framework clearly support the ion-exchange properties of seidite-(Ce). Presumably, all the extra-framework ions and H_2O groups are guests that can be removed from the host structure through the described system of pores. The minimum and maximum effective widths of the two types of eight-membered channels described above are about 3 and 5 Å, respectively; the same widths are about 1 and 6.5 Å in the ten-membered channels, the bottleneck corresponding to two facing Ti octahedra (Fig. 15).

Modular aspects

The (100) layer consisting of eight-membered channels that occur in seidite-(Ce) (Fig. 15) is well known as a double layer of corner-sharing Si tetrahedra, and is present in the structures listed in Table 3 (cf. Rocha and Lin 2005). In all these compounds, the silicate double layer alternates with a sheet of cations that mainly show an octahedral coordination.

Variety of tetrahedral and "octahedral" sheets. The tetrahedral sheets forming the double layers are comparable with the so-called apophyllite sheet, which consists of a net of four-membered rings connected to form eight-membered rings. However, taking into account the orientation of the tetrahedra in the four-membered rings, three types of tetrahedral sheets can be distinguished (Fig. 17): all tetrahedra pointing either upwards or downwards (apophyllite); three tetrahedra pointing upwards and one downwards [all the compounds of Table 3 except seidite-(Ce)]; two tetrahedra pointing upwards and two downwards [seidite-(Ce)]. Cavansite [$Ca(VO)Si_4O_{10}\cdot 4H_2O$; *Pcmn*, $a = 9.792$, $b = 13.644$, $c = 9.629$ Å; Evans 1973] has a seidite-(Ce)-like tetrahedral sheet but the two tetrahedra pointing in the same direction share a corner instead of occupying opposite sides of a four-membered ring.

Five types of "octahedral" sheets occur in the compounds of Table 3 (Fig. 18).

- Isolated Ti octahedra in seidite-(Ce) (Fig. 15).
- Chains of edge-sharing Ca octahedra in rhodesite (Figs. 16, 18a), macdonaldite and hydrodelhayelite. This sheet corresponds to a trioctahedral sheet where one out of two chains of octahedra is missing.

Table 3. Members of the rhodesite mero-plesiotype series.

Name	*Chemical formula*	*a*, *b*, *c* (Å), β (°)	*S.G.*	*Ref.*
Seidite-(Ce)	$Na_4(Ce,Sr)_2\{Ti(OH)_2(Si_8O_{18})\}(O,OH,F)_4\cdot 5H_2O$	24.61, 7.23,14.53, 94.6	*C*2/*c*	(1)
Rhodesite	$K_2Ca_4[Si_8O_{18}(OH)]_2\cdot 12H_2O$	23.416, 6.555, 7.050	*Pmam*	(2)
Macdonaldite	$BaCa_4[Si_8O_{18}(OH)]_2\cdot 10H_2O$	14.081, 13.109, 23.560	*Cmcm*	(3)
Delhayelite	$K_7Na_3Ca_5[Si_7AlO_{19}]_2F_4Cl_2$	24.86, 7.07, 6.53	*Pmmn*	(4)
Hydrodelhayelite	$K_2Ca_4[Si_7AlO_{17}(OH)_2]_2\cdot 6H_2O$	6.648, 23.846, 7.073	$Pnm2_1$	(5)
Monteregianite-(Y)	$K_2Na_4Y_2[Si_8O_{19}]_2\cdot 10H_2O$ *	9.512, 23.956, 9.617, 93.85	$P2_1/n$	(6)
AV-9	$K_2Na_4Eu_2[Si_8O_{19}]_2.10H_2O$ **	23.973, 14.040, 6.567, 90.35	*C*2/*m*	(7)

* $K_2Na_4Ce_2[Si_8O_{19}]_2\cdot 10H_2O$ (AV-5 in Rocha et al. 2000) is isostructural with monteregianite-(Y).

** Isostructural compounds with Tb (Ananias et al. 2001), Er (Ananias et al. 2004) and Nd (Rocha et al. 2004) substituting Eu are known.

References: (1) Ferraris et al. 2003; (2) Hesse et al. 1992; (3) Cannillo et al. 1968; (4) Cannillo et al. 1970; (5) Ragimov et al. 1980; (6) Ghose et al. 1987; (7) Ananias et al. 2001

- Chains of alternating Y and Na octahedra connected by pairs of further Na octahedra, to form a trioctahedral sheet with vacancies, in monteregianite-(Y) and its isostructural compound with Ce substituting Y (Fig. 18b).
- A trioctahedral-like sheet in delhayelite (Fig. 18c), where edge-sharing chains like those of rhodesite alternate with chains of eight-coordinated Na-polyhedra.
- A modification of the sheet of monteregianite-(Y) in the AV-9 compounds (Fig. 18d), where the coordination number of the inter-chain Na-polyhedra is 9. This type of sheet requires that two H_2O molecules per formula unit, which in other structures of the group reside in the channels, move to the coordination sphere of Na within the "octahedral" sheet.

The Na atoms that belong to the "octahedral" sheet and have coordination number higher than six also bind to bridging oxygen atoms of the silicate double layer. Thus, these Na atoms are in contact with the channels and leaching can be favored, as it has been described above for the heterophyllosilicate delindeite.

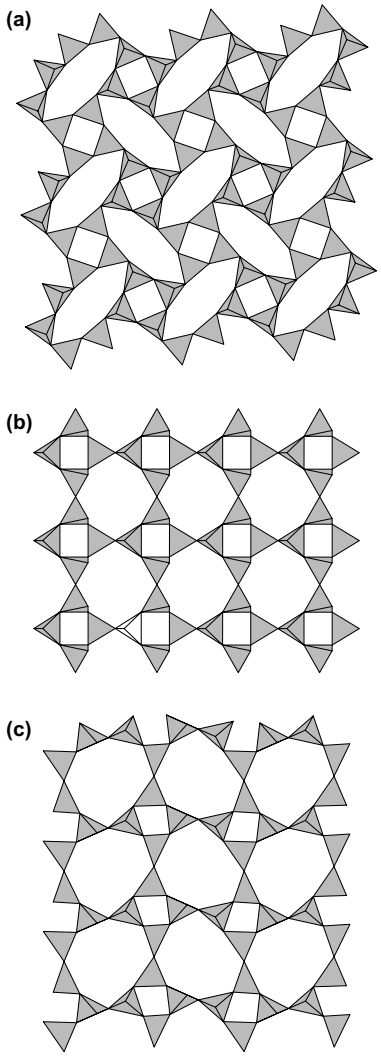

Figure 17. Tetrahedral sheets in apophyllite (a), rhodesite (b) and seidite-(Ce) (c).

The rhodesite mero-plesiotype series. According to the categorization of modular series given by Makovicky (1997) (cf. Ferraris et al. 2004), the compounds of Table 3 form a mero-plesiotype series (cf. footnote 1). In fact, nearly the same double silicate layer occurs in all members and alternates with a variable module (merotype aspect). The series is also plesiotypic because, as seen above, the silicate double layer may show a different ratio between upwards and downwards pointing tetrahedra. This aspect is related to the number, charge and coordination number of the cations in the interlayer sheet and to the Si/Al ratio within the layer. Most of the compounds in Table 3 have a *T*:O ratio of 8:19 (*T* = Si, Al), corresponding to a 3:1 ratio between the tetrahedra sharing three and four corners, respectively. In seidite-(Ce), the ratio between the two types of tetrahedra is 1:1, consequently *T*:O = 8:18; the different connectivity of the tetrahedra is related to the relative shift between the two apophyllite-type sheets forming the double silicate layer. As mentioned above, depending on this shift, the lateral view of the double layer shows either five- (Fig. 15) or eight-membered rings (Fig. 16).

Further modular interpretation. The porous structures of the rhodesite series and those related to this series (see next section) can be described as based on *OTT* layers and compared with the 1:1 (*TO*) and 2:1 (*TOT*) layer silicates and the heterophyllosilicates. The two facing

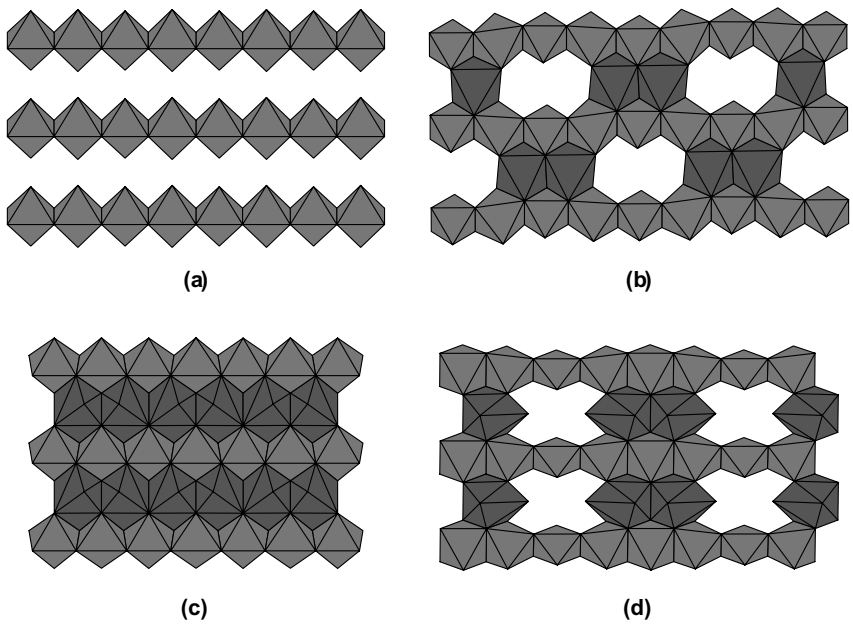

Figure 18. "Octahedral" sheets in rhodesite (a), monteregianite-(Y) (b), delhayelaite (c) and AV-9 (d). The Na polyhedra (dark grey) joining parallel rows of edge-sharing octahedra (light grey) have coordination number 6, 8, and 9 in (b), (c) and (d), respectively.

T sheets, which present two types of rings instead of one only as in the 1:1 and 2:1 silicates, are joined by sharing apical corners of tetrahedra to form the porous *TT* layer. The formal *O* sheet is by far more variable than in the layer silicates and connects two adjacent *TT* sheets; thus, a three-dimensional framework is formed without weaker bonds between the formal *OTT* layers.

Structures related to the rhodesite series

Reyerite and fedorite. These two minerals belong to the group of gyrolite, $Ca_{16}NaSi_{23}AlO_{60}(OH)_8 \cdot 14H_2O$, which is extensively described in this volume by Bonaccorsi and Merlino (2005), and are members of a merotype series (cf. Ferraris et al. 2004). A double tetrahedral layer consisting of eight-membered rings and comparable to that described for the rhodesite group occurs in reyerite, $Ca_{14}(Na,K)_2Si_{22}Al_2O_{58}(OH)_8 \cdot 6H_2O$, and fedorite, $[K_2(Ca_5Na_2)Si_{16}O_{38}(OH,F)_2 \cdot H_2O$, (Fig. 19). The minimum effective channel width is about 3 Å in both structures. In fedorite, the double layer alternates with a trioctahedral sheet of Ca octahedra, thus reinforcing similarity with the rhodesite group. However, the two equivalent silicate sheets forming the double layer do not display the apophyllite-type but consist of two types of six-membered rings; one type is quite deformed.

A heterophyllosilicate H sheet in jonesite. The partially disordered crystal structure of jonesite $\{Ba_2(K,Na)[Ti_2(Si_5Al)O_{18}(H_2O)] \cdot (H_2O)_n$; $a = 8.694$, $b = 25.918$, $c = 8.694$ Å, $\beta = 104.73°$, $P2_1/m$; Krivovichev and Armbruster 2004$\}$ shows a double layer forming [100] eight-membered channels (Fig. 20) similar to those described for the rhodesite series. However, the (010) sheet delimiting the double layer has the same chemical composition and topology of the *H* sheet typical of the *HOH* bafertisite-type layer (Fig. 3): some of the silicate tetrahedra are substituted by Ti octahedra. The minimum effective width of the pores is about 3.3 Å.

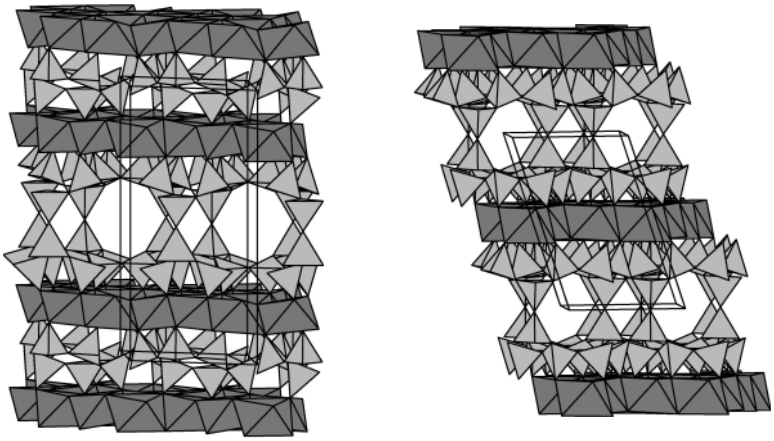

Figure 19. Crystal structure of reyerite (a) seen along [010] (*c* axis vertical) and fedorite seen along [100] (b).

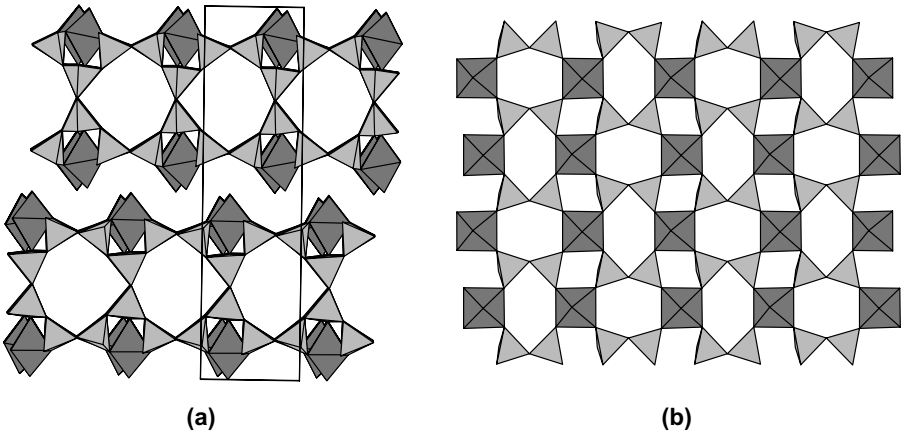

Figure 20. Jonesite: (010) double layer seen along [100] (a); (010) projection of the bafertisite-type *H* sheet (b) delimiting the double layer.

Analogues of seidite-(Ce). Ermolaeva et al. (2005) describe a new phase from the Lovozero and Khibina massifs that has chemical composition (Th,REE)(Ti,Nb)(Si,P)$O_6{\cdot}n H_2O$ and is supposed to be an analog of seidite-(Ce) with Th > REE. This phase occurs with bitumen-like substances whose formation from light hydrocarbons (like methane) is likely catalyzed by the presence of microporous heterosilicates. At the same time, the transformation of metal organic complexes occurring in the bitumen-like substances leads to the formation of microphases of Ti- and Nb-silicates of Th, Ca, Ln, Y, Na and K (cf. Chukanov and Pekov 2005). On the basis of the chemical formula, the latter authors suppose that also the amorphous mineral umbozerite, $Na_3Sr_4Th(Mn,Zn,Fe)Si_8O_{24}(OH)$ (Es'kova et al. 1974), is an analog of seidite-(Ce).

CONCLUSIONS

Modularity (Ferraris et al. 2004) is a common crystallographic feature of the microporous structures presented in this and other chapters of this volume. In itself, this aspect is not important for the investigation of microporous properties but, as in general holds for modular structures, can be crucial in the process of modeling the structures of new microporous phases related to others already known. Thus, modularity may be a tool useful to solve difficult structures.

Modularity can also inspire paths towards the synthesis of tailored microporous compounds, for example by playing on the type and stacking of modules, according to well established patterns widely documented in modular materials. Instructive under this aspect, are the members of the mero-plesiotype series for which it is possible to play on a variable module and on the specific configurations of the modules to introduce useful properties, as described in this volume by Rocha and Lin (2005) for compounds of the rhodesite series.

In principle, as already Nature does, the *HOH* layer of the heterophyllosilicates can be exploited to build materials with a variety of interlayer contents. Besides, following some indications of swelling observed in the field, presumably pillared materials can be prepared by using *HOH* layers; the presence of Ti polyhedra both in the *H* and *O* sheets might be useful for applications in heterogeneous catalysis. However, whereas the microporous structures described in the sections on palysepioles and rhodesite series are well known to materials scientists and several of them are promising for technological applications, the porous properties occurring in some heterophyllosilicates are active in nature, but still unknown and unexploited in the world of technology.

ACKNOWLEDGMENTS

The authors are indebted with N.V. Chukanov for communicating unpublished IR data and constructively reading the manuscript and to Peter Nèmeth for useful discussions on aspects of the heterophyllosilicates. Research supported by MIUR (Rome) as the FIRB project “Properties and technological applications of minerals and their synthetic analogues” and the PRIN project “Microstructural and modular aspects in minerals: analyses and applications.”

REFERENCES

Ananias D, Ferreira A, Rocha J, Ferreira P, Rainho JP, Morais C, Carlos LD (2001) Novel microporous europium and terbium silicates. J Am Chem Soc 123:5735-5742

Ananias D, Rainho JP, Ferreira A, Rocha J, Carlos LD (2004) The first examples of X-ray phosphors, and C-band infrared emitters based on microporous lanthanide silicates. J Alloys Compd 374:219-222

Anderson JA, Galan-Fereres M (1999) Precursor-support interactions in the preparation of sepiolite-supported Ni and Pd catalysts. Clay Minerals 34:57-66

Artioli G, Galli E (1994) The crystal structures of orthorhombic and monoclinic palygorskite. Mater Sci Forum 166-169:647-652

Bellezza M, Franzini M, Larsen AO, Merlino S, Perchiazzi N (2004) Grenmarite, a new member of the götzenite-seidozerite-rosenbuschite group from the Langesundsfjord district, Norway: definition and crystal structure. Eur J Mineral 16:971-978

Belov NV, Gavrilova GS, Solov’eva LP, Khalilov AD (1978) The refined structure of lomonosovite. Sov Phys Dokl 22:422-424

Bonaccorsi E, Merlino S (2005) Modular microporous minerals: cancrinite-davyne group and C-S-H phases. Rev Mineral Geochem 57:241-290

Brauner K, Preisinger A (1956) Struktur und Entstehung des Sepioliths. Tsch Mineral Petrogr Mitt 6:120-140

Burke EAJ, Ferraris G (2004) New minerals and nomenclature modifications approved in 2003 by the Commission on New Minerals and Mineral Names, International Mineralogical Association. Can Mineral 42:905-913

Camara F, Garvie LAJ, Devouard B, Groy TL, Buseck PR (2002) The structure of Mn-rich tuperssuatsiaite: a palygorskite-related mineral. Am Mineral 87:1458-1463
Cannillo E, Rossi G, Ungaretti L (1970) The crystal structure of delhayelite. Rend Soc Ital Miner Petrol 26: 63-75
Cannillo E, Rossi G, Ungaretti L, Carobbi SG (1968) The crystal structure of macdonaldite. Atti Accad Naz Lincei, Classe Sci Fisiche 45:399-414
Casal B, Merino J, Serratosa JM, Ruiz Hitzky E (2001) Sepiolite-based materials for the photo- and thermal-stabilization of pesticides. Appl Clay Sci 18:245-254
Chahi A, Petit S, Decarreau A (2002) Infrared evidence of dioctahedral-trioctahedral site occupancy in palygorskite. Clays Clay Mineral 50:306-313
Chelishchev NF (1972) Ion-exchange properties of astrophyllites under supercritical conditions. Geokhimiya 7:856-860 (in Russian)
Chelishchev NF (1973) Ion exchange properties of minerals. Nauka, Moscow (in Russian)
Chernov AN, Ilyukhin VV, Maksimov BA, Belov NV (1971) Crystal structure of innelite, $Na_2Ba_3(Ba,K,Mn)(Ca,Na)Ti(TiO_2)_2[Si_2O_7]_2(SO_4)_2$. Sov Phys Crystallogr 16:87-92
Chiari G, Giustetto R, Ricchiardi G (2003) Crystal structure refinements of palygorskite and Maya Blue from molecular modelling and powder synchrotron diffraction. Eur J Mineral 15:21-33
Christiansen CC, Johnsen O, Makovicky E (2003) Crystal chemistry of the rosenbuschite group. Can Mineral 41:1203-1224
Christiansen CC, Makovicky E, Johnsen ON (1999) Homology and typism in heterophyllosilicates: an alternative approach. N Jb Mineral Abh 175:153-189
Christiansen CC, Rønsbo JG (2000) On the structural relationship between götzenite and rinkite. N Jb Mineral Mh 2000:496-506
Chukanov NV, Pekov IV (2005) Heterosilicates with tetrahedral-octahedral frameworks: mineralogical and crystal-chemical aspects. Rev Mineral Geochem 57:105-144
Chukanova VN, Pekov IV, Chukanov NV, Zadov AE (2002) Iron-rich analogue of sepiolite and the conditions of its formation in the contact aureole of the Lovozero alkaline massif. Geochem Intern 40:1225-1229
Colville AA, Anderson CP, Black PM (1971) Refinement of the crystal structure of apophyllite: I. X-ray diffraction and physical properties. Am Mineral 56:1222-1233
Cool P, Vansant EF, Poncelet G, Schoonheydt RA (2002) Layered structures and pillared layered structures. *In*: Handbook of porous solids. Vol 1. Schüth F, Sing KSW, Weitkamp J (eds) Wiley-VCH, p 1251-1310
Corma A (1997) From microporous to mesoporous molecular sieve materials and use in catalysis. Chem Rev 97:2373-2419
Corma A, Garcia H, Leyva A, Primo A (2004) Alkali-exchanged sepiolites containing palladium as bifunctional (basic sites and noble metal) catalysts for the Heck and Suzuki reactions. Appl Catal A 257:77-83
Egorov-Tismenko YuK (1998) Polysomatic series of seidozerite-nacaphite minerals of titanosilicate mica analogues. Crystallogr Rep 43:306-312
Egorov-Tismenko YuK, Sokolova EV (1990) Structural mineralogy of the homologic series seidozerite-nacaphite. Mineral Zh 12(4):40-49 (in Russian)
Ercit TS, Cooper MA, Hawthorne FC (1998) The crystal structure of vuonnemite, $Na_{11}Nb_2(Si_2O_7)(PO_4)_2O_3(F,OH)$, a phosphate-bearing sorosilicate of the lomonosovite group. Can Mineral 36:1311-1320
Ermolaeva VN, Chukanov NV, Pekov IV, Nekrasov AN, Sokolov SV, Kogarko LN (2005) On the role of organic substances in transport and concentration of thorium and other rare elements in alkaline pegmatites of Lovozero and Khibiny peralkaline massifs. Geochem Intern (in press)
Es'kova YeM, Semenov YeI, Khomyakov AP, Mer'kov AN, Lebedeva SI, Dubakina LS (1974) Umbozerite, a new mineral. Dokl Akad Sci USSR, Earth Sci 216:124-126
Espantaleón AG, Nieto JA, Fernandez M, Marsal A (2003) Use of activated clays in the removal of dyes and surfactants from tannery waste waters. Appl Clay Sci 24:105-110
Evans HT Jr (1973) The crystal structures of cavansite and pentagonite. Am Mineral 58:412-424
Fahey JJ, Ross, M, Axelrod JM (1960) Loughlinite, a new hydrous sodium magnesium silicate. Am Mineral 45:270-281
Fernandez-Saavedra R, Aranda P, Ruiz-Hitzky E (2004) Templated synthesis of carbon nanofibers from polyacrylonitrile using sepiolite. Adv Functional Mater 14:77-82
Ferraris G (1997) Polysomatism as a tool for correlating properties and structure. EMU Notes Mineral 1: 275-295
Ferraris G (2004) Are the HOH layers of the heterophyllosilicates suitable to prepare pillared materials? Acta Crystallogr A60:s53
Ferraris G, Belluso E, Gula A, Khomyakov, AP, Soboleva SV (2003) The crystal structure of seidite-(Ce), $Na_4(Ce,Sr)_2\{Ti(OH)_2(Si_8O_{18})\}(O,OH,F)_4\cdot 5H_2O$, a modular microporous titanosilicate of the rhodesite group. Can Mineral 41:1183-1192

Ferraris G, Belluso E, Gula A, Soboleva SV, Ageeva OA, Borutskii BE (2001a) A structural model of the layer titanosilicate bornemanite based on seidozerite and lomonosovite modules. Can Mineral 39:1665-1673

Ferraris G, Ivaldi G, Khomyakov AP, Soboleva SV, Belluso E, Pavese A (1996) Nafertisite, a layer titanosilicate member of a polysomatic series including mica. Eur J Mineral 8:241-249

Ferraris G, Ivaldi G, Pushcharovsky DYu, Zubkova NV, Pekov IV (2001b) The crystal structure of delindeite, $Ba_2\{(Na,K,\square)_3(Ti,Fe)[Ti_2(O,OH)_4Si_4O_{14}](H_2O,OH)_2\}$, a member of the mero-plesiotype bafertisite series. Can Mineral 39:1307-1316

Ferraris G, Khomyakov AP, Belluso E, Soboleva SV (1997) Polysomatic relationship in some titanosilicates occurring in the hyperagpaitic alkaline rocks of the Kola Peninsula, Russia. Proc 30th Inter Geol Cong 16:17-27

Ferraris G, Khomyakov AP, Belluso E, Soboleva SV (1998) Kalifersite, a new alkaline silicate from Kola Peninsula (Russia) based on a palygorskite-sepiolite polysomatic series. Eur J Mineral 10:865-874

Ferraris G, Makovicky E, Merlino S (2004) Crystallography of Modular Materials. IUCr Monographs in Crystallography, Oxford University Press, Oxford

Ferraris G, Nèmeth P (2003) Pseudo-symmetry, twinning and structural disorder in layer titanosilicates. Abstracts of ECM-21 (Durban), p 41

Galan E (1996) Properties and applications of palygorskite-sepiolite clays. Clay Minerals 31:443-453

Galan E, Carretero I (1999) A new approach to compositional limits for sepiolite and palygorskite. Clays Clay Mineral 47:399-409

Galan E, Ferrero F (1982) Palygorskite-sepiolite clays of Lebrija, Southern Spain. Clays Clay Mineral 30: 191-199

García Romero E, Suárez Barrios M, Bustillo Revuelta MA (2004) Characteristics of a Mg-palygorskite in Miocene rocks, Madrid Basin (Spain). Clays Clay Mineral 52:484-494

Garcia Sanchez A, Alvarez Ayuso E, Jimenez de Blas O (1999) Sorption of heavy metals from industrial waste water by low-cost mineral silicates. Clay Minerals 34:469-477

Ghose S, Sen Gupta PK, Campana CF (1987) Symmetry and crystal structure of monteregianite, $Na_4F_2Y_2Si_6O_{38}\cdot 10H_2O$, a double-sheet silicate with zeolitic properties. Am Mineral 72:365-374

Giustetto R, Chiari G (2004) Crystal structure refinement of palygorskite from neutron powder diffraction. Eur J Mineral 16:521-532

Grice JD (1991) The crystal structure of silinaite, $NaLiSi_2O_5\cdot 2H_2O$: a monophyllosilicate. Can Mineral 29: 363-367

Guan YaS, Simonov VI, Belov NV (1963) Crystal structure of bafertisite, $BaFe_2TiO[Si_2O_7](OH)_2$. Dokl Akad Sci 149:123-126 (published 1965)

Guggenheim S, Eggleton RA (1988) Crystal chemistry, classification, and identification of modulated layer silicates. Rev Mineral 19:675-725

Güven N (1988) Smectites. Rev Mineral 19:497-559

Hejny C, Armbruster T (2001) Polytypism in xonotlite $Ca_6Si_6O_{17}(OH)_2$. Z Kristallogr 216:396-408

Hesse KF, Liebau F, Merlino S (1992) Crystal structure of rhodesite, $HK_{1-x}Na_{x+2y}Ca_{2-y}$ $\{lB,3,2^2_\infty\}$ $[Si_8O_{19}]\cdot(6\text{-}z)H_2O$, from three localities and its relation to other silicates with dreier double layers. Z Kristallogr 199:25-48

Hong W, Fu P (1982) Jinshajiangite—a new Ba-Mn-Fe-Ti-bearing silicate mineral. Geochemistry (China) 1: 458-464 (in Chinese)

Jones BF, Galan E (1988) Sepiolite and palygorskite. Rev Mineral 19:631-674

Khomyakov AP (1995) Mineralogy of hyperagpaitic alkaline rocks. Clarendon Press, Oxford

Khomyakov AP (2004) Zeolite-like amphoterosilicates of hyperagpaitic rocks and their unique properties. Micro-and Mesoporous Mineral Phases (Accad Lincei, Roma), Volume of Abstracts, p 231-234

Khomyakov AP, Ferraris G, Belluso E, Britvin SN, Nechelyustov GN, Soboleva SV (1998) Seidite-(Ce), $Na_4SrCeTiSi_8O_{22}F\cdot 5H_2O$—a new mineral with zeolite properties. Zap Vseross Mineral Obs 127(4):94-100 (in Russian)

Khomyakov AP, Ferraris G, Nechelyustov GN, Ivaldi G, Soboleva SV (1995) Nafertisite $Na_3(Fe^{3+}, Fe^{2+})_6[Ti_2Si_{12}O_{34}](O,OH)_7\cdot 2H_2O$, a new mineral with a new type of band silicate radical. Zap Vseross Mineral Obs 124(6):101-108 (in Russian)

Khomyakov AP, Nechelyustov GN, Sokolova EV, Dorokhova GI (1992) Quadruphite $Na_{14}CaMgTi_4[Si_2O_7]_2[PO_4]_2O_4F_2$ and polyphite $Na_{17}Ca_3Mg(Ti,Mn)_4[Si_2O_7]_2[PO_4]_6O_2F_6$, two new minerals of the lomonosovite group. Zap Vseross Mineral Obs 121(3):105-112 (in Russian)

Krivovichev SV, Armbruster T (2004) The crystal structure of jonesite, $Ba_2(K,Na)[Ti_2(Si_5Al)O_{18}(H_2O)](H_2O)_n$: A first example of titanosilicate with porous double layers. Am Mineral 89:314-318

Krivovichev SV, Yakovenchuk VN, Armbruster T, Döbelin N, Pattison P, Weber HP, Depmeier W (2004) Porous titanosilicate nanorods in the structure of yuksporite, $(Sr,Ba)_2K_4(Ca,Na)_{14}(\square,Mn,Fe)\{(Ti,Nb)_4(O,OH)_4[Si_6O_{17}]_2[Si_2O_7]_3\}(H_2O,OH)_n$, resolved using synchrotron radiation. Am Mineral 89:1561-1565

Kuang W, Facey GA, Detellier C (2004) Dehydration and rehydration of palygorskite and the influence of water on the nanopores. Clays Clay Mineral 52:635-642

Louis M, Guillemin CJ, Goni JC, Ragot JP (1968) Coloration rose-carmin d'une sepiolite eocene, la quincyte, par des pigments organiques. *In:* Advances in Organic Geochemistry 1968. Schenck PA, Havenaar I (eds) Pergamon Press, p 553-566

Makovicky E (1997) Modularity – different types and approaches. EMU Notes Mineral 1:315-344

Makovicky E, Karup-Møller S (1981) Crystalline steenstrupine from Tunugdliarfik in the Ilímaussaq alkaline intrusion, South Greenland. N Jb Mineral Abh 140:300-330

Martin-Vivaldi JL, Linares-Gonzales J (1962) A random intergrowth of sepiolite and attapulgite. Clays Clay Mineral 9:592-602

Massa W, Yakubovich OV, Kireev VV, Mel'nikov OK (2000) Crystal structure of a new vanadate variety in the lomonosovite group: $Na_5Ti_2O_2[Si_2O_7](VO_4)$. Solid State Sci 2:615-623

Matsubara S (1980) The crystal structure of orthoericssonite. Mineral J 10:107-121

McCusker LB (2005) IUPAC nomenclature for ordered microporous and mesoporous materials and its application to non-zeolite microporous mineral phases. Rev Mineral Geochem 57:1-16

McCusker LB, Liebau F, Engelhardt G (2003) Nomenclature of structural and compositional characteristics of ordered microporous and mesoporous materials with inorganic hosts (IUPAC recommendations 2001). Microporous Mesoporous Mater 58:3-13

McDonald AM, Grice JD, Chao GY (2000) The crystal structure of yoshimuraite, a layered Ba-Mn-Ti silicophosphate, with comments of five-coordinated Ti^{4+}. Can Mineral 38:649-656

Mellini M, Ferraris G, Compagnoni R (1985) Carlosturanite: HRTEM evidence of a polysomatic series including serpentine. Am Mineral 70:773-781

Men'shikov YuP, Khomyakov AP, Polezhaeva LI, Rastsvetaeva RK (1996) Shkatulkaite, $Na_{10}MnTi_3Nb_3(Si_2O_7)_6(OH)_2F{\cdot}12H_2O$: a new mineral. Zap Vseross Mineral Obs 125(1):120-126 (in Russian)

Men'shikov YuP, Khomyakov AP, Ferraris G, Belluso E, Gula A, Kulchitskaya EA (2003) Eveslogite, $(Ca,K,Na,Sr,Ba)_{24}[(Ti,Nb,Fe,Mn)_6(OH)_6Si_{24}O_{72}](F,OH,Cl)_7$, a new mineral from the Khibina alkaline massif, Kola Peninsula, Russia. Zap Vseross Mineral Obs 132(1):59-67 (in Russian)

Merlino S (ed) (1997) Modular aspects of minerals. EMU Notes in Mineralogy. Vol 1. Budapest, Eötvös University Press

Merlino S, Pasero M, Khomyakov AP (1990) The crystal structure of lintisite, $Na_3LiTi_2(Si_2O_6)_2O_2{\cdot}2H_2O$, a new titanosilicate from Lovozero (USSR). Z Kristallogr 193:137-148

Mizutani T, Fukushima Y, Okada A, Kamigaito O (1991) Hydrothermal synthesis of sepiolite. Clay Minerals 26:441-445

Moore PB (1971) Ericssonite and orthoericssonite. Two new members of the lamprophyllite group, from Lånbgan, Sweden. Lithos 4:137-145

Nèmeth P (2004) Characterization of new mineral phases belonging to the heterophyllosilicate series. Doctorate Dissertation, Dipartimento di Scienze Mineralogiche e Petrologiche, Università di Torino

Nèmeth P, Ferraris G, Dódony I, Radnóczi G, Khomyakov AP (2004a) Models of the modular structures of two new heterophyllosilicates related to bornemanite and barytolamprophyllite. Acta Cryst A60:s196

Nèmeth P, Ferraris G, Radnóczi G, Ageeva OA (2005) TEM and X-ray study of syntactic intergrowths of epistolite, murmanite and shkatulkalite. Can Mineral, in press

Nèmeth P, Gula A, Ferraris G (2004b) Towards pillared heterophyllosilicates? Suggestions from nature. Micro- and Mesoporous Mineral Phases (Accad Lincei, Roma), Volume of Abstracts, p 265-267

Pekov IV, Chukanov NV (2005) Microporous framework silicate minerals with rare and transition elements: minerogenetic aspects. Rev Mineral Geochem 57:145-172

Pekov IV, Chukanov NV, Ferraris G, Ivaldi G, Pushcharovsky DYu, Zadov AE (2003) Shirokshinite, $K(NaMg_2)Si_4O_{10}F_2$, a new mica with octahedral Na from Khibiny massif, Kola Peninsula: descriptive data and structural disorder. Eur J Mineral 15:447-454

Pen ZZ, Shen TC (1963) Crystal structure of bafertisiste, a new mineral from China. Sci Sin 12:278-280 (in Russian)

Pen ZZ, Zhang J, Shu J (1984) The crystal structure of barytolamprophyllite. Kexue Tongbao 29:237-241

Perrault G, Harvey Y, Pertsowsky R (1975) La yofortierite, un nouveau silicate hydraté de manganèse de St-Hilaire, P.Q. Can Mineral 13:68-74

Petersen OV, Johnsen O, Christiansen CC, Robinson GW, Niedermayr G (1999) Nafertisite - $Na_3Fe_{10}Ti_2Si_{12}(O,OH,F)_{43}$ - from the Nanna Pegmatite, Narsaarsuup Qaava, South Greenland. N Jb Mineral Mh 1999:303-310

Piilonen PC, Lalonde AE, McDonald AM, Gault RA, Larsen AO (2003a) Insights into astrophyllite-group minerals. I. Nomenclature, composition and development of a standardized general formula. Can Mineral 41:1-26

Piilonen PC, McDonald AM, Lalonde AE (2003b) Insights into astrophyllite-group minerals. II. Crystal chemistry. Can Mineral 41:27-54

Prowse WG, Arnot KI, Recka JA, Thomson RH, Maxwell JR (1991) The quincyte pigments—fossil quinones in an eocene clay mineral. Tetrahedron 47:1095-1108

Pushcharovsky DYu, Pasero M, Merlino S, Vladykin NV, Zubkova NV, Gobechiya ER (2002) Crystal structure of zirconium-rich seidozerite. Crystallogr Rep 47:196-200

Pushcharovsky DYu, Pekov IV, Pluth J, Smith J, Ferraris G, Vinogradova SA, Arakcheeva AV, Soboleva SV, Semenov EI (1999) Raite, manganonordite-(Ce) and ferronordite-(Ce) from Lovozero massif: crystal structures and mineral geochemistry. Crystallogr Rep 44:565-574

Putnis A (2002) Mineral replacement reactions: from macroscopic observations to microscopic mechanisms. Mineral Mag 66:689-708

Ragimov Kg, Chiragov MI, Mamedov KS, Dorfman MD (1980) Crystal structure of hydrodelhayelite, $KH_2Ca(Si,Al)_8O_{19}{\cdot}H_2O$. Dokl Akad Nauk Azerbaid SSR 36:49-51 (in Russian)

Rastsvetaeva RK (1998) Crystal structure of betalomonosovite from the Lovozero region. Sov Phys Crystallogr 31:633-636

Rastsvetaeva RK, Chukanov NV (1999) Crystal structure of a new high-barium analogue of lamprophyllite with a primitive unit cell. Doklady Chemistry 368(4-6):228-231

Rastsvetaeva RK, Sokolova MN Gusev AI (1990) Refined crystal structure of lamprophyllite. Mineral Zh 12(5):25-28 (in Russian)

Rastsvetaeva RK, Tamazyan RA, Sokolova EV, Belakovskii DI (1991) Crystal structures of two modifications of natural Ba,Mn-titanosilicate. Sov Phys Crystallogr 36:186-189

Rocha J, Anderson MW (2000) Microporous titanosilicates and other novel mixed octahedral-tetrahedral framework oxides. E J Inorg Chem 2000:801-818

Rocha J, Carlos LD, Ferreira A, Rainho J, Ananias D, Lin Z (2004) Novel microporous and layered luminescent lanthanide silicates. Mater Sci Forum 455-456:527-531

Rocha J, Lin Z (2005) Microporous mixed octahedral-pentahedral-tetrahedral framework silicates. Rev Mineral Geochem 57:173-202

Rozenberg KA, Rastsvetaeva RK, Verin IA (2003) Crystal structure of surkhobite: new mineral from the family of titanosilicate micas. Crystallogr Rep 48:384-389

Rytwo G, Tropp D, Serban C (2002) Adsorption of diquat, paraquat and methyl green on sepiolite: experimental results and model calculations. Appl Clay Sci 20:273-282

Schoonheydt RA, Pinnavaia T, Lagaly G, Gangas N (1999) Pillared clays and pillared layered solids. Pure Appl Chem 71:2367-2371

Scott JD (1976) Crystal structure of miserite, a Zoltai type 5 structure. Can Mineral 14:515-528

Semenov EI, Organova NI, Kukharchik MV (1962) New data on minerals of the lomonosovite-murmanite group. Sov Phys Crystallogr 6:746-751

Shariatmadari H, Mermut AR, Benke MB (1999) Sorption of selected cationic and neutral organic molecules on palygorskite and sepiolite. Clays Clay Mineral 47:44-53

Shi N, Ma Z, Li G, Yamnova NA, Pushcharovsky DYu (1998) Structure refinement of monoclinic astrophyllite. Acta Crystallogr B54:109-114

Singer A, Huang PM (1989) Adsorption of humic acid by palygorskite and sepiolite. Clay Minerals 24:561-564

Sokolova E, Hawthorne FC (2001) The crystal chemistry of the $[M_3\Phi_{11-14}]$ trimeric structures from hyperagpaitic complexes to saline lakes. Can Mineral 39:1275-1294

Sokolova E, Hawthorne FC (2004) The crystal chemistry of epistolite. Can Mineral 42:797-806

Sokolova EV, Egorov-Tismenko YuK, Khomyakov AP (1987) Special features of the crystal structure of $Na_{14}CaMgTi_4[Si_2O_7]_2[PO_4]_2O_4F_2$ - homologue of sulphohalite and lomonosovite structure types. Mineral Zh 9(3):28-35 (in Russian)

Sokolova EV, Egorov-Tismenko YuK, Khomyakov AP (1988) Crystal structure of sobolevite. Sov Phys Dokl 33:711-714

Sokolova EV, Egorov-Tismenko YuK, Khomyakov AP (1989a) The crystal structure of nacaphite. Sov Phys Dokl 34:9-11

Sokolova EV, Egorov-Tismenko YuK, Pautov LA, Belakovskii DI (1989b) Structure of the natural barium titanosilicate $BaMn_2TiO[Si_2O_7](OH)_2$, a member of the seidozerite-nacaphite homologous series. Zap Vses Mineral Obs 118(4):81-84 (in Russian)

Springer G (1976) Falcondoite, nickel analogue of sepiolite. Can Mineral 14:407-409

Thompson JB Jr (1978) Biopyriboles and polysomatic series. Am Mineral 63:239-249

Ustinov VI, Ul'yanov AA (1999) Intrastructural isotopic investigation of the transformation of minerals with a layered structure. Geochem Intern 37:908-911

Veblen DR (1991) Polysomatism and polysomatic series: A review and applications. Am Mineral 76:801-826

Veblen DR, Buseck PR (1979) Chain-width order and disorder in biopyriboles. Am Mineral 64:687-700

Velde B (1992) Introduction to clay minerals. Chapman & Hall, London

Vrána S, Rieder M, Gunter ME (1992) Hejtmanite, a manganese-dominant analogue of bafertisite, a new mineral. Eur J Mineral 4:35-43

Woodrow PJ (1967) The crystal structure of astrophyllite. Acta Crystallogr 22:673-678

Yamnova NA, Egorov-Tismenko YuK, Khomyakov AP (1996) Crystal structure of a new natural (Na,Mn,Ti)-phyllosilicate. Crystallogr Rep 41:239-244

Yamnova NA, Egorov-Tismenko YuK, Pekov IV (1998) Crystal structure of perraultite from the Coastal Region of the Sea of Azov. Crystallogr Rep 43:401-410

Yang Z, Cressey G, Welch M (1999) Reappraisal of the space group of bafertisite. Powder Diffraction 14: 22-24

Zaitsev VA, Krigman LD, Kogarko LN (2004) Pseudobinary phase diagram lamprophyllite-nepheline. Lithos 73(1-2):s122

Zhou K, Rastsvetaeva RK, Khomyakov AP, Ma Z, Shi N (2002) Crystal structure of new micalike titanosilicate – Bussenite, $Na_2Ba_2Fe^{2+}[TiSi_2O_7][CO_3]O(OH)(H_2O)F$. Crystallogr Rep 47:50-53